Stine Arctander

Condition Assessment of Hydro Generator Stator Bar Insulation

Examination of PD void activity versus AC voltage magnitude and frequency.

Master's thesis

NTNU
Norwegian University of Science and Technology
Faculty of Information Technology and Electrical Engineering
Department of Electric Power Engineering

NTNU
Norwegian University of
Science and Technology

Stine Arctander

Condition Assessment of Hydro Generator Stator Bar Insulation

Examination of PD void activity versus AC voltage magnitude and frequency.

NTNU
Norwegian University of
Science and Technology

Preface

This Master's Thesis is the final work for the Masters program in Electric Power Engineering at the Norwegian University of Science and Technology (NTNU) in Trondheim. The thesis has been completed during the spring semester of 2020 and equals to 30 ECTS-credits. I would like to thank my supervisor, Prof. Erling Ildstad for help and support during my work.

I would also give my thanks to my co-supervisor Doctor Torstein Grav Aakre, for the help with the experimental lab setup and for being able to help me with the thesis structure and questions during a complicated time due to the Covid-19 situation. I would also like to thank Espen Eberg at Sintef for the generator rod samples used for the experimental part of this thesis.

Trondheim, 30th June, 2020

Stine Arctander

Abstract

The introduction of weather dependent renewable energy to the existing grid is affecting the current operating pattern of electricity production. When combining energy sources like PV and wind power to power production from hydro power, the operation is controlled with more starts and stops, and at a heavier load than known before. It is inevitable that this affects the condition of the generator, however in what degree this transition will be harmful for hydro generators over time is not clear. This makes proper diagnostic testing and condition assessment valuable to increase the lifetime of hydro generators.

The main purpose of this thesis is to address the concerning issues using partial techniques for detection of internal critical voids in high voltage insulation. The aim is considering the effect of high voltage AC testing at very low frequencies to 50Hz both theoretically and experimentally.

A literature survey is given together with the theory to provide a basis for the work presented in the results and discussion. There are two parts to this thesis, one theoretical analysis of PD characteristics and one experimental laboratory test for a set of stator rods testing their PD characteristics considering PDIV/PDEV and charge magnitude.

For the theoretical part a cylindrical and spherical void has been simulated for their electric field with an increasing void length and gap distance in a FEM-tool. As the gap-length relation decreases, the field is close to homogeneous with no present edge effect for the void with 0.2mm gap distance and 2mm length due to the very high field throughout the field. The edge effect had a small increase in terms of total area affected as the void grew smaller, and no noticeable difference was proven with void lengths bigger than 10mm. The magnitude of the electric field at the very corners increased along with an increasing length when the gap distance was fixed.

The electric field of a spherical void was equal to the theoretical limitation for voids under 10mm diameter, when the total insulation thickness increased accordingly. With a fixed insulation thickness and the void diameter increasing, a deviation from the theory was seen already when the void diameter exceeded 1/3 of the insulation thickness by 1mm. A frequency dependency was proven for the cylindrical voids under very low frequencies. A 14% deviation in PDIV for a 2.2mm void was observed for a VLF of 10^{-6} compared to at 50Hz.

In the experimental laboratory tests, two service aged near HV and 2 back-up stator rods from a Norwegian run-of-the-river power plant was tested.

One of the back-up rods proved a PDIV of 50% of the average of the 3 other rods tested. The peak operating voltage for the rods were 1.9kV, while the PDIV was 500V under this limit. The average of the three rods with equal PDIV/PDEV levels could be approximated to the theoretical estimation of PDIV, where a void of 1.9mm could cause the equal PDIV in the rods. Rod, S2, with a low PDIV did not fit the theoretical model.

The average charge magnitude for rod S2 and R2 were both dependent on the frequency and the PDIV level. The average charge magnitude was 87% higher for the service rod than the back-up rod at 50Hz.

Sammendrag

Innføringen av væravhengige fornybare energikilde i det eksisterende nettet vil påvirke det nåværende driftsmønsteret fra strømproduksjon vi kjenner i dag. Når man kombinerer energikilder som sol- og vindkraft med kraftproduksjon fra vannkraft, blir driften endret hvor maskiner blir utsatt for flere start og stopp, samtidig som det kjøres med en tyngre last. Det er uunngåelig at dette påvirker tilstanden til generatorer, men i hvilken grad denne overgangen i kjøremønsteret er skadelig for vannkraftsgeneratorer over tid er ikke kjent. Dette gjør det nødvendig å ha tilstrekkelig diagnostikk og tilstands analyse tilgjengelig for å forlenge levetiden til generatorene. Hensikten med denne oppgaven er å adressere problemstillingen rundt PD analyse, og bruke tilgjengelige metoder for påvisning og karakterisering av partielle utladninger i høyspennings isolasjon. Målet er å vurdere effekten av høyspenning AC-testing ved veldig lave frekvenser og opp til 50Hz både teoretisk og eksperimentelt.

En litteraturstudie og teoretisk bakgrunn er presentert som et grunnlag for arbeidet som presenteres i resultat og diskusjon. Det er to deler til denne oppgaven, en teoretisk analyse av PD-egenskaper og et eksperimentelt forsøk for et sett med generator staver for å undersøke PD-egenskaper med tanke på PDIV/PDEV og utladningsstørrelse. For den teoretiske delen har det blitt simulert et sylindrisk og sfærisk hulrom for å undersøke endringen i det elektriske feltet ved økende hulromslengde og bredde med FEM-simulering. Når lengde/bredde forholdet avtar, er feltet nær homogent uten tilsynelatende kanteffekt for hulrommet med 0.2mm bredde og 2mm lengde fordi det svært høye feltet er påvist gjennom hele hulrommet. Kanteffekten hadde en liten økning av det totale arealet som ble påvirket da hulrommet ble mindre, denne effekten avtok ved hulrom over 10mm.

Det maksimale feltet i hjørnene økte sammen med en økende lengde av hulrommet ved konstant bredde. Det elektriske feltet til et sfærisk hulrom var lik den teoretiske ligningen for hulrom under 10mm i diameter, da den totale isolasjonstykkelsen økte tilsvarende. Ved måling under konstant isolasjonstykkelse for sfærisk hulrom med endring i lengde, ble det oppdaget avvik fra teorien da hulrommets diameter overskred 1/3 av isolasjonstykkelsen allerede ved 1mm. En frekvensavhengighet ble påvist for de sylindriske hulrommene under svært lave frekvenser. Et avvik på 14% i PDIV for et hulrom på 2.2mm ble observert for en VLF på 10^{-6} sammenlignet med ved 50Hz.

I de eksperimentelle laboratorieundersøkelsene ble det testet to brukte generatorstaver fra nær HV terminal og to tilsvarende ubrukte back-up staver. En av back-up stavene viste en PDIV på 50% av gjennomsnittet av de tre andre test-objektene. Under maksimal spenning i drift har stavene blitt utsatt for en spenning på 1.9kV, mens PDIV viste 500V under denne grensen. Gjennomsnittet av de tre stavene med like PDIV/PDEV-nivåer kunne tilnærme seg den teoretiske estimeringen av PDIV, der et hulrom på 1.9mm forårsaket den samme PDIV verdien som i test objektene.

Gjennomsnittlig utladningsstørrelse for stav S2 og R2 var begge avhengig av frekvensen og PDIV-nivået. Gjennomsnittlig utladningsstørrelse var 87% høyere for den brukte staven S2, enn back-up staven R2.

Contents

List of Figures

List of Tables

1 Introduction

1.1 Background

The Norwegian powermarkets has a long history of using hydropower as their main source for electric energy, and 94% of all power production today comes from hydro power. Around 1626 hydroelectric power stations are installed throughout the country, and one third of the power production comes from plants installed before 1970. As these hydro generators have been in service for over 40 years, they are expected to soon have reached their expected lifetime and are in need for refurbishment or replacement [3].

Today, power production in general is becoming influenced by the integration of other renewable sources like solar and wind power. When integrating such weather dependent renewable resources into the hydro power production, the production is operated with more frequent starts and stops along with a heavier operation load than before. Before integrating renewable resources, hydrogenerators could operate below their maximum nominal load, in order to extend its lifetime [4]. It is not yet clear in what degree this transition is harmful for the hydrogenerators, and how it will affect their service lifetime. This creates a need for useful diagnostic testing and condition assessment methodology for hydro generators.

In 2009 the Cigre working group A1.10 published an international survey describing statistical information conducting hydrogenerator failures [5]. Norway contributed in this survey with 34% of the total generators analysed, and was the main contributor of machines. The results of the survey shows that of all incidents reported, 62% was failures connected to insulation damage. Of all stator faults during the survey, 70% was related to PD activity in the stator insulation. The survey stated that of all failures studied, the most important one is insulation failure because of the damage it can cause the generator performance. With this in mind, there is a need for diagnostic testing and clear criteria for analysing PD activity as the power system today is exposed to more complex operating stresses which it was not designed for originally, as large farms of renewable resources are on a rise.

Electrical partial discharge measurements are one of the most common tools used today for condition assessment for stator insulation [6] [7]. When applied to a test object, the results can be analysed in order to conclude about the condition of the object. When performing electrical PD testing under normal frequency, 50Hz, the test equipment can be massive of size, like the coupling capacitor and the power source. By using lower frequencies, the test setup components can be minimised in order to facilitate for PD testing out in the field. However, the main challenges that is faced today is that there is a need for educated experience within PD testing to be able to supply for sensible conclusions about the condition of the test object.

The properties of PD occurance in the insulation is harmful for the generator, exposing it for potential breakdown or irreversible damage. With this knowledge it is of great importance that there exist an effective condition assessment and knowledge of PD characteristics, and that is the main motivation for this thesis.

1.1.1 Peaking Power - Weather Dependent Renewable Resources

Traditionally the operating pattern of hydropower generation has been planned to operate in a constant mode, where starts and stops have been kept to a minimum. As the power market now is becoming more internationalised and deregulated, new operation procedures for starting and stopping the power production in order to sell and buy power at the most favorable prices are proven beneficial. Because of the change in operation and load conditions, many power plants are now operating under conditions witch they were not intended to operate under. According to Statkraft 2008, there was a triplication of start-stop in hydropower plants from 1993-2000, and further a doubling from 2001-2003 [8]. With this change, excessive wear on technical components for the power production are inevitable. High temperatures in the generator windings as well as voltage transients are risk the generator is vulnerable to due to peaking power operation. It is of interest for power facilities to understand the degree of degradation of their equipment due to these operating changes, in order to maximise their earnings.

1.2 Aim and Approach

The initial intention for this thesis was to have a experimental objective for a thoroughly condition assessment and characteristics of a set of service aged generator rods and their equal back-up rods with respect to frequency and temperature. Because of the Covid-19 pandemic schools and labs closed down and the author was forced to change the thesis objective mid March. An alternative theoretical approach to PD-characteristics was proposed and constitutes one part of this thesis. As the labs opened up sooner than expected, parts of the initial experimental objective was performed and constitutes the other part of this thesis.

The theoretical part is focused on simulations using both FEM tools and the theoretical simulation of the ABC-model, and the second part is a practical approach for PD testing of generator rods. The theoretical part is a study of how the electrical field with edge effects is affected by change of the void dimensions. The void has been modelled with both a cylindrical and a spherical shape for the same insulation permittivity and voltage. A theoretical analysis of the same cylindrical void dimensions have been conducted in a ABC-model to analyse how the inception and extinction voltage is affected when various frequencies is applied. The same frequency study has been performed experimentally on samples of generator rods from a river hydropower plant. Both rods that have been in service and their equal back-up rods have been tested in a range of frequencies to study the change in PDIV end PDEV. By comparing the results from the theoretical and experimental study the intention is to analyse how the PDIV differs from a theoretical perspective, and hopefully also an estimation of the total size of the voids present during PDIV in the service aged generator rods.

1.3 Hydro Generators - Stator Rods

Different winding orientations in hydro generators are usually chosen based on the final power output. For large hydro generators with a power output of >50MVA, half turn coils called roebel bars are most commonly used [6]. By using a bar shape, the insertion of large the windings is more manageable. The materials in a generator bars usually consist of a mica and epoxy mix as insulation material, and a mica tape surrounding the outer part of the bar [1].
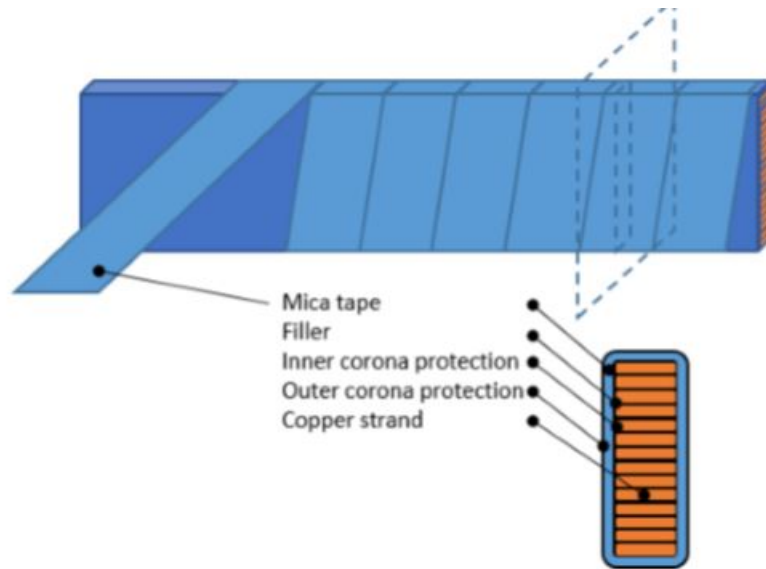
Figure 1: General structure of a Roebel bar [1]

Insulation of Generator Rods

The insulation in generator rods is usually differentiated between the groundwall-, turn- and strand insulation, in terms of categorizing voids occurrence. The rods used for the practical part of this thesis did not have turn insulation, and therefor it is not described further. The strand insulation surrounds every single copper strand inside the bar, while the groundwall insulation separates the copper conductors from the grounded core, illustrated in Figure 2.
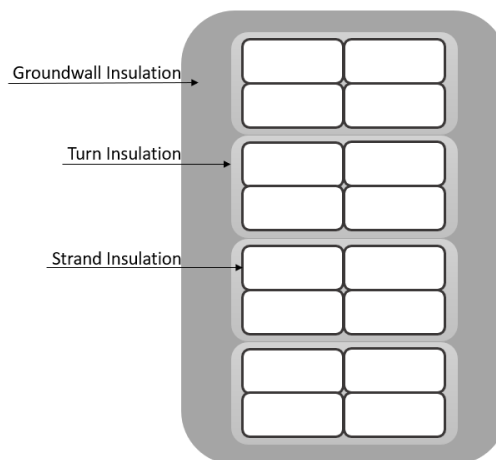
Figure 2: Insulation mechanisms in Roebel bars

The formation of a cavity within the groundwall insulation a critical for the quality of the rod insulation. Usually due to a void or cavity, a ground fault relay can cause complete failure of the winding, forcing production to shut down immediately. In order for the equipment to maintain a long life time in service, it is critical for the insulation to be able to withstand a number of stress factors like electrical, thermal and mechanical forces, discussed further in chapter 1.4. A Roebel bar will have the same groundwall insulation thickness throughout the rod, making it convenient to reverse their position in the stator in order to extend the rods life time [6]. Meaning, the end formerly placed at neutral can now be placed at the phase end exposing it for high voltage.

The groundwall insulation is also exposed to increased ambient temperature. This makes the thermal resistance of the insulation material especially important in order to prevent high temperatures in the copper conductors. The groundwall should have high thermal conductivity, with no cavities present. When cavities are present in the groundwall, they will block the heat flow in the insulation and can cause thermal faults.

The currents flowing at respectively the top and bottom for every stator bar, creating two magnetic fields acting on the copper conductors causing vibration. The force acting on the top of a bar at 120Hz for a 60Hz current in radial direction for a Roebel bar at 1m length can be described by [6]:

$$F = \frac{cI^2}{d}KN/m \tag{1}$$

I is the rms current, d is the stator sloth width in meters and c is 0.96 constant. Together with the radial force, the magnetic field of the generator rotor creating a circumferential force which interacts with the magnetic field caused by the current in the stator bars. The circumferential force is close to 10% of the total radial force [6]. By knowing this, we can see the importance of having an insulation without cavities in order for the conductors to not move around freely, causing insulation abrasion.

1.4 Deterioration Mechanisms

The authors specialisation project was concerned with the same topic as this master thesis, and no new information was to be added to the background theory concerning deterioration mechanisms. This chapter is thus based from the work completed in advance.

There are several types of deteriorating mechanisms that can affect the condition of the insulation for generator windings. These stresses are known by the name "TEAM" stresses, which include thermal, electrical, ambient and mechanical stresses. Each of these stresses can either be applied constantly to the equipment or they can appear as a transient, meaning only occurring for a short period of time. Examples of transient sources can be lightning strikes, switching and out-of-phase synchronization of generators. If a machine fails because of constant stress, its time to failure is equal to the number of total operating hours. If a machine fails due to a transient, its time to failure is equal to the number of transients that has occurred.

Thermal Stress
One of the most important stress factors to acknowledge is degradation due to the operating temperature of the windings. There are several sources that can increase this temperature, like eddy currents, I^2R losses, stray load losses in the conductors and losses in the core like windage. The influence of temperature increasing sources is dependent on

the design and functioning of the machine in general.

Degradation due to thermal stress is usually classified within either oxidation stress or thermomechanical stress. Due to oxidation of the insulation, where it has been exposed to increasing temperature over a period of time, it can cause the insulation to dry, leaving it brittle and can cause delamination of the groundwall and strand tape layers. As this is a first order chemical reaction the lifetime (Hours) of the insulation as a function of temperature (Kelvin) can be given by The Dakin/Arrhenius rate law

$$L = Ae^{\frac{B}{T}} \tag{2}$$

where A and B are constants. However, it is important to state that this reaction is only valid for temperatures over a certain threshold, as well as there are a number of other chemical reactions occurring at the same time that must be taken into consideration.

Larger rotating machines are also subject to thermomechanical stresses due to fast load changes, and off/on switching. Because the thermal expansion coefficients are different for conductors and insulation, a rapid temperature change can cause great thermal change between the materials. Delamination and an increasing $\tan\delta$ can also occur due to thermomechanical stress [7].

Electrical stress

When designing high voltage stator windings, the insulation is mainly determined by the electrical stress, given by

$$E = \frac{V}{d}[kV/mm] \tag{3}$$

where E is electrical stress, V is applied power frequency voltage and d is the distance (mm).

If air-filled cavities or voids appear in the insulation, partial discharges will take place during service. If this fault is not corrected, it can erode through the groundwall insulation, causing a complete failure for the stator winding. To represent the lifetime of the insulation when there is known PD activity, the inverse power model is often used

$$L = cE^{-}n \tag{4}$$

where L in the lifetime (h), c is a constant, E is the electric stress applied over the insulation and n is the power law constant. Usually the power law constant is in the range 9-12, this means if we assume n=10, the lifetime of the machine will be shortened by 1000times if the electric stress is doubled [6].

Electrical stress is equal to the thermal stress considering that below a certain threshold there is no aging of the insulation. For electrical stress this threshold is defined as the partial extinction voltage (DEV).

Ambient Stress

Ambient stresses is triggered by factors from the surrounding environment to the rotating machines. Normally these factors alone will not cause aging, but combined with other TEAM stress factors, it can cause abrasion of stator insulation. Examples of ambient stresses is [6]

- Moisture from condensed on the windings

- High humidity

- Aggressive chemicals

- Abrasive particles in the cooling air

- Pollution from the environment, such as insects, fly ash, coal dust, and powders that are by-products of associated industrial processes (cement, pulp, chemical residues, etc.)

Mechanical Stress
Stator generator rods can be exposed to mechanical stress by a magnetic force oscillating at twice the power frequency. The relationship between this mechanical force and the currentflow in a stator bar is given by

$$F = \frac{cI^2}{d} kN/m \qquad (5)$$

where F is the force acting on the top of the coil at 120Hz for a 60Hz current in radial direction for 1m length, I is the RMS current, d is the width of the stator slot (m) and c is a constant.

If the stator bars are not tightened properly, this force can cause the bars to vibrate in their slot causing groundwall abrasion. A similar force can be applied to the end winding, if the bars are free to vibrate relative to each other, or blocking and support rings, this can also cause insulation abrasion. In comparison with the model for thermal and electrical stress, there is no such model acknowledged for mechanical stress. However, there are some models describing the amount of abrasion occurring, but they are not practical and yet none have become a basis for standard accelerated aging test under vibration [9].

2 Theory

Parts of this chapters is based from the authors previous work concerning the same topics, in the specialisation project submitted fall 2019. Content that is from work that is not the authors, is properly acknowledged.

2.1 Partial Discharges

The appearance of insulation faults like voids or cavities in high voltage equipment can be the source of electrically discharges that only partially bridges the insulation between the conductors. The gaseous voids within the insulation achieves a higher electric stress than the solid insulation surrounding it, while its dielectric strength is weakened. In IEEE standard 1434 partial discharge is defined as "*An electrical discharge that only partially bridges the insulation between conductors. A transient gaseous ionization occurs in an insulation system when the electric stress exceeds a critical value, and this ionization produces partial discharges* [10]".

Due to the high local electric stress, an electrical breakdown of the air in the voids can cause a spark which can degrade the insulation. This can make the fault erode completely through the groundwall insulation causing a complete failure if it is not corrected. If a complete breakdown of the insulation have taken place, the stator rod needs to be re-wound or replaced with a back-up bar, meaning the machine is needed to be taken out of service. Because of the damaging properties of partial discharges, it is a very important aging mechanism for a number of various high voltage equipment.

Partial discharges is normally distinguished in terms of the insulation interface, as it can occur in gases, liquid and solid interfaces.

2.1.1 Partial Discharges in Stator Bar Insulation

In solid dielectrics like in Roebel bars insulation, air filled voids can appear. The electric field within the voids will be enhanced for the zero-crossing of the applied voltage. This leads to discharges occurring early in the phase, as well as the number if discharges occurring is increased [11]. When the electric field stress inside the void exceeds the insulation dielectric strength, together with an available start electron, the breakdown of the air can cause a degrading spark. The electric field in a flat void is perpendicular to the applied electric field shown by

$$E_{void} = \epsilon_r \cdot E \tag{6}$$

ϵ_r is the relative permittivity of the insulation material. The most common insulation material today is usually made of mica and epoxy resin, and has a relative permittivity of about 4 [4]. E is the electric field in an insulation material with no cavities. For spherical cavities the maximum electric field stress is described by:

$$E_h = \frac{3\epsilon_r}{1 + 2\epsilon_r} \cdot E \tag{7}$$

ϵ_r is the relative permittivity of the insulation material. The field enhancement has a maximum relation of 1.5 times higher than the field strength in the surrounding insulation material.

The electric strength of the air inside a cavity can be determined by the Paschen Curve. From Paschen's Law we know that the dimensions of the void and air pressure are critical parameters. When PDs occur in the insulation, they are repeated once every half-cycle, as a minimum [2]. PDs are able to gradually deteriorate the insulation until a complete puncture occurs, and the winding is short-circuited. Three ways of deterioration is described in TET4160-Digital compendium for Insulation material for high voltage applications by Erling Ildstad. [2].

First is bombardment by ions and electrons on the insulation around the cavity area.

Second, it can be due to a chemical reaction caused by the discharges and an elevated temperature. This is particularly true for organic materials.

Third, discharges emits radiation, which ultraviolet radiation has sufficient energy to break chemical bonds in organic materials. Because small PDs cannot be observed with human senses, as larger ones can be visible or audible to some extent, there is a need for sensitive measuring methods.

2.1.2 Offline Detection of PD

Detecting PDs in high voltage equipment can be done with several methods like online or offline electric testing, visual detection, audible testing or by testing for known by-products like ozone created by discharges in insulation. Some of these test demands equipment to be partial or fully dissembled like offline tests, while the others can be performed to some extent during regular machine operation. When testing the insulation strength, the machine usually needs to be taken out of service.

In order to detect PDs, devices sensitive to high frequencies is used. Usually big capacitors 80-1000pF are sufficient for electrical testing, and it is connected in parallel to the

test object. It is necessary that the windings tested is energized with minimum its phase-to-ground rating using a high voltage source for discharges to form, this is applicable for both VLF and LF ranges also.

PD diagnostic testing in stators windings is described in details in standards IEEE-1434 and IEC 60034-27-1. When doing electrical PD testing for stator windings the PD magnitude is commonly higher in the initial phase of voltage application, This is due to a build up of space charges and gas pressure in the cavities. By gradually increasing the applied voltage this source of error can be avoided.

The PDIV tells us at what voltage level the discharges occurs, and PDEV at what voltage level the discharges are no longer detectable when the voltage is decreasing. In a perfect functioning machine both PDIV and PDEV should be above its service voltage level, meaning no discharges are present. Another test parameter to analyse is the peak magnitude of PDs, Q_m. The peak magnitude is measurable because of a small current flowing at each PD occurring, this is due to electrons and ions flowing in the gas filled cavities for every single PD that occurs. The current that is flowing will then be regulated by a fixed value of pico Coulombs(pC) by the charge. By measuring the voltage pulse across the impedance created by the current flowing, it will represent the magnitude of PDs [6]. Using a PD(PRPD) analyzer for electrical PD testing, we are able to record PD magnitude, phase positions of the PD and exactly how many PDs are occurring. With the phase resolved PD analysis it is also possible to study the PD patterns in order to identify what type of defect is causing discharges. However, there is no clear standards on how to interpret the PRPD patterns but several studies have been done on this topic.

2.2   ABC-Equivalent Model

Assuming the insulation system is purely capacitive, a capacitive equivalent circuit can be made in order to study partial discharges in high voltage insulation. The ABC-equivalent circuit shown in Figure 3 consist of three different capacities, where capacitance c is representing a void in the insulation, b is the insulation which is in series with the void, and a represents the capacitance for the remaining insulation. For the justification of this theoretical model, some assumptions needs to be made. First of all, the void and the high voltage insulation can be modelled like proposed in the ABC-circuit. It also needs to be assumed that there is only one void where partial discharges is occurring, and that the current in the external circuit is equal to zero when a discharge is occurring, usually for 10ns [2].
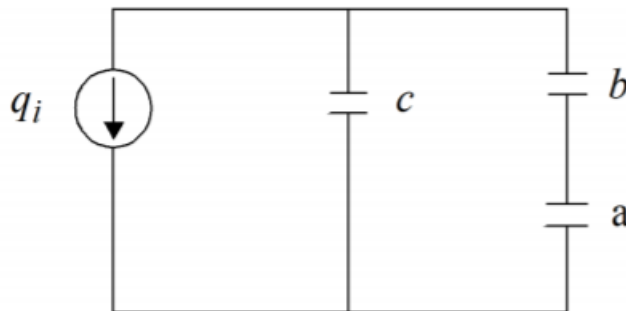

Figure 3: ABC-Equivalent Circuit

When using an abc-equivalent circuit to model voids, both quantities and magnitudes

of partial discharges can be found by electrical measurements. During a discharge the ignition voltage(Us0) will fall to a remanent voltage(Ur0). The charge q_i injected across the void of a magnitude that cause the voltage to drop can be seen in relation to the drop in ignition voltage.

$$\Delta U = U_{s0} - U_{r0} \tag{8}$$

The charge injected across capacitance c is proven by

$$q_i = \Delta U(c + \frac{ab}{a+b}) \approx \Delta U(b+c) = (U_{s0} - U_{r0})(b+c) \tag{9}$$

The charge injected can not directly be measured by the external circuit. There will be a small drop in the voltage level across capacitance a

$$\Delta u_a = \frac{b}{a+b} \cdot \Delta U \approx \frac{b}{a} \cdot \Delta U \tag{10}$$

When the voltage drops occurs, after the discharges have extinguished, a transient current from the external circuit is able to restore the voltage level back to its original level. By measuring this current, it will represent the charge of the discharge occurring. The assumption that in a real insulation system capacitance a>>c and c>b, the expression for the apparent charge can be simplified further.

$$q_a = \Delta u_a \cdot (a + \frac{bc}{b+c}) \approx \Delta u_a \cdot a \approx b \cdot \Delta U = b(U_{s0} - U_{r0}) \tag{11}$$

q_a, the apparent charge is in this case the magnitude of the total discharges occurring. This means that this charge is equal to the charge transferred to the test object from the external circuit, in order to restore the voltage level which will drop under the occurrence of a partial discharge [2].

2.3   AC Voltage Application

When AC voltage is applied to the test object, the voltage across the cavity under no partial discharge occurrence can be estimated with

$$u_{c0}(t) = \frac{b}{b+c}\sqrt{2}U\sin\omega t \tag{12}$$

where b and c is the representative capacitance's found in the ABC-equivalent model, and U is the applied voltage.

A discharge will occur under AC voltage when the voltage across the insulation void exceeds the breakdown strength of air. This will cause the ignition voltage to decrease to the remanent voltage, showed in Figure 4. After the drop in voltage, the voltage level will reset to the same level as before the discharge happened. The numbers of PD occurring is increasing per half-cycle of the voltage.

The voltage decreases by ΔU after reaching U_{s0} after a PD occurrence, gives

$$u_1(t) = \frac{b}{b+c}\sqrt{2}U\sin\omega t - (U_{s0} - U_{r0}), t_1 < t < t_2 \tag{13}$$

After this the voltage will go back to its initial level after the discharge have extinguished very fast. With the assumption that discharges only happens when the voltage level peaks, the number of discharges can be calculated by

$$n = \frac{2(\frac{b}{b+c}\sqrt{2}U - U_{r0})}{U_{s0} - U_{r0}} \tag{14}$$
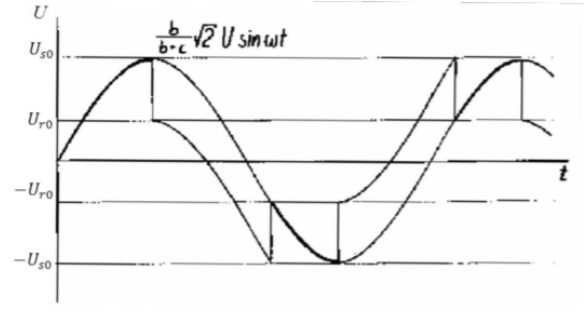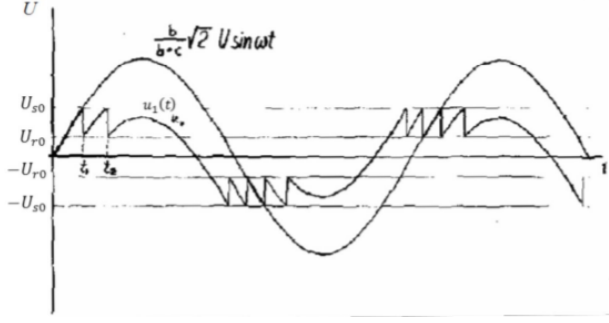
9

Figure 4: PDs occurring after reaching PDIV [2]   Figure 5: PDs occurring at PDIV moment [2]

Discharges will occur in a test object when the voltage level reaches its PD occurrence threshold, PDIV. The relation of the inception voltage, U_i, and the ignition voltage U_{s0} is shown with

$$U_{s0} = \sqrt{2}U_i \cdot \frac{b}{b+c} \tag{15}$$

$$U_i = \frac{b+c}{b} \cdot \frac{U_{s0}}{\sqrt{2}} \tag{16}$$

b and c are the capacitance's from the abc-model. When the voltage level have reached PDIV, the voltage can be reduced slightly without the extinction of the discharges. This will first happen when the voltage applied have reached its extinction voltage, U_e. When the voltage level is right at the extinction voltage, it is assumed that one discharge is occurring at every peak of the voltage [2].

2.3.1 Frequency Dependency

Testing stator bars under power frequency requires a large voltage source combined with a transformer in order to energise the large capacitor and test object. In some cases it is advantageous to perform PD condition analysis at the generator locations, rather than to deconstruct the machine and transport the equipment to a test facility. By energising high voltage equipment with very low frequency(VLF), the voltage source can be significantly smaller and easier to apply and bring along for service purposes.

By expanding the capacitive ABC-equivalent circuit with resistors, a frequency dependent circuit can be modelled. Material conductivity is also applied in this model, and facilitate for studying the change of void voltage in relation to a range of temperatures. This circuit will yield a relation between applied voltage and the voltage in the void, which is frequency dependent [12] [13].
The mechanisms representing the void in the insulation is denoted with subscript c, the insulation with subscript b and the resistance and dielectric response added to the insulation is denoted with subscript a.
Assuming a cylindrical void in the insulation the relationship of the applied voltage U_i and the voltage across the void U_s can be proven by Eq.17

$$U_i = (1 + \frac{d_b}{d_c} \cdot \frac{\sigma_c + j\omega\epsilon_0\epsilon_{r,c}}{\sigma_b + j\omega\epsilon_0\epsilon_{r,b}}) \cdot U_s \tag{17}$$

10
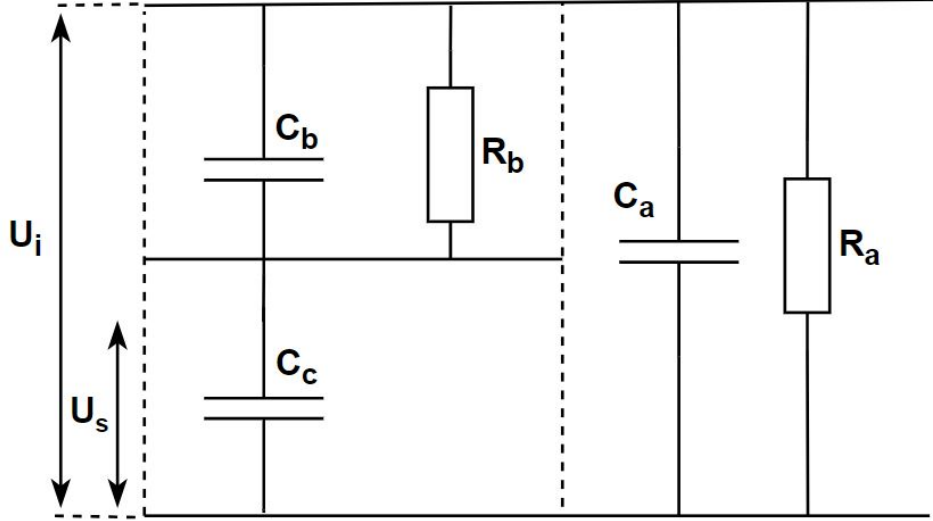
Figure 6: Capacitive and resistive ABC-model

where d_b is the thickness of the insulation which is in parallel with the void, d_c is the distance of the void, σ_b is the insulation conductivity, σ_c is conductivity of the air inside the void. Normally $sigma_c$ can be assumed close to zero, and it is thereafter neglected for the tests in this thesis. $\epsilon_0 \epsilon_{r.c}$ is relative permittivity of vacuum and air, $\epsilon_{r,b}$ is the permittivity of the insulation material and ω is the angular frequency of $2\pi f$ where f is the frequency.

By considering the electric field inside the void homogeneous, we can use Paschen Law to understand the withstand strength of the air inside the void [12] [2]. This is assuming that partial discharges occur on a basis when the voltage across the void is greater than the withstand strength of air. PDIV can be estimated by using the Paschen curve:

$$U_s = 6.72\sqrt{pd} + 24.36(pd)[kV] \qquad (18)$$

p is the pressure times d the distance, ranging from 10^{-2} to $5{\cdot}10^2$ bar cm.
The ABC circuit can be expanded further to include the dielectric response. This analyses the dielectric loss by polarisation relaxation mechanisms in a material. An in depth analysis if this can already be found in T.Aakre 2020 [4].

3 Method

3.1 FEM Analytics of Electrical Fields in Voids

Modelling of voids high voltage insulation is performed with the model in Figure 7. The model is adapted from a previous NTNU master thesis "Condition Assessment of Hydro Generator Insulation Using Partial Discharge Measurements" by Regina Skattenborg 2018.

There are two copper electrodes surrounding the test samples, both cylindrical where the high voltage electrode has a diameter of 30mm and the ground electrode has a diameter of 90mm.

A high voltage of $V_{Peak} = \sqrt{2} \cdot 7kV$ is applied from the upper high voltage electrode, while the bottom electrode is grounded. The HV electrode is surrounded by epoxy with $\epsilon_r = 4.2$. The high voltage insulation around the cavity is polycarbonate with $\epsilon_r = 3.4$
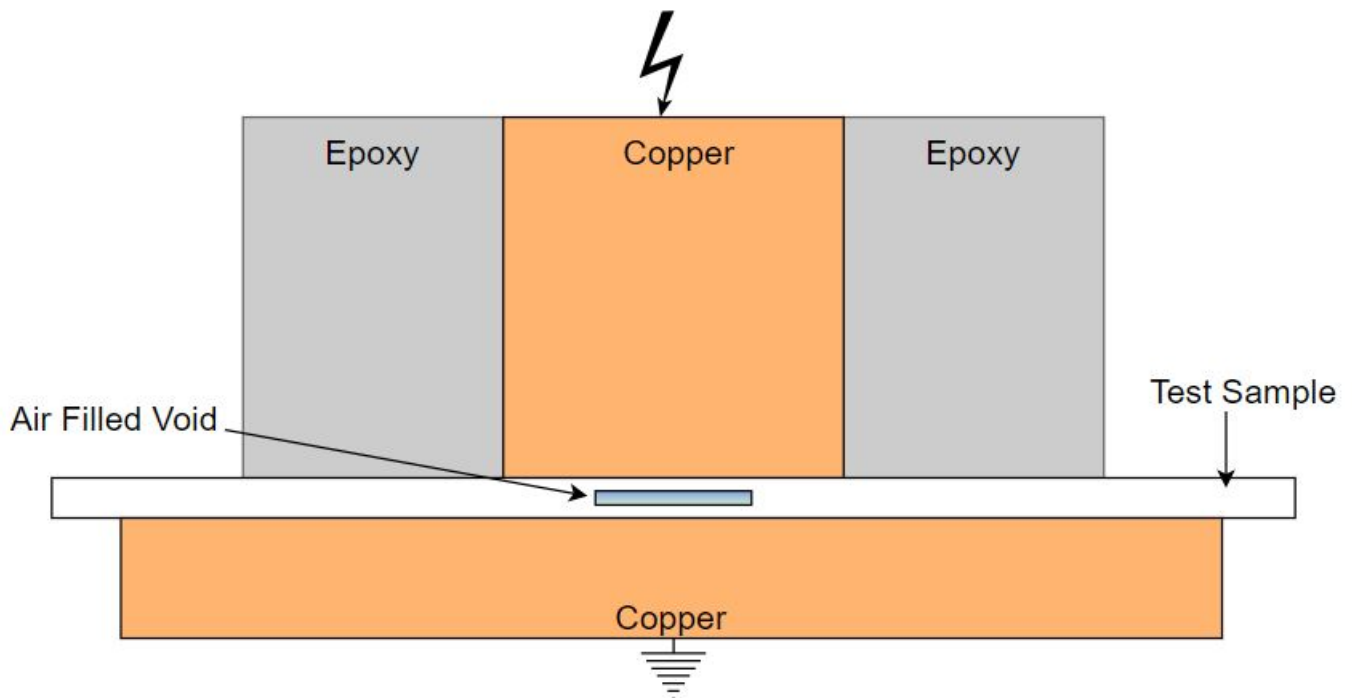
Figure 7: The FEM-analytical model visualised with its domains and materials

3.1.1 Geometry

The model is made as a 2D axisymmetric model along y axis. All domains are made of rectangles, which will present a cylindrical model with the axisymmetri. The entire model is encapsulated in an area filled with air. The gap distance and the void length is varied throughout the test. The insulation thickness is changed accordingly with changed gap distances. This means the final gap distance of the void will never be larger than $1/3$ of the total insulation material. For the spherical void shape the insulation thickness is both kept constant when the diameter is increasing and increased accordingly with the void diameter. It is interesting to find at what spherical void diameter to insulation thickness ratio the electrical field is no longer homogeneous. For this simulation the insulation thickness was kept at 2mm for each layer, while the void diameter increased so its size exceeded all three insulation layers. Both models for a cylindrical and spherical shape is presented in Figure 8 and 9.
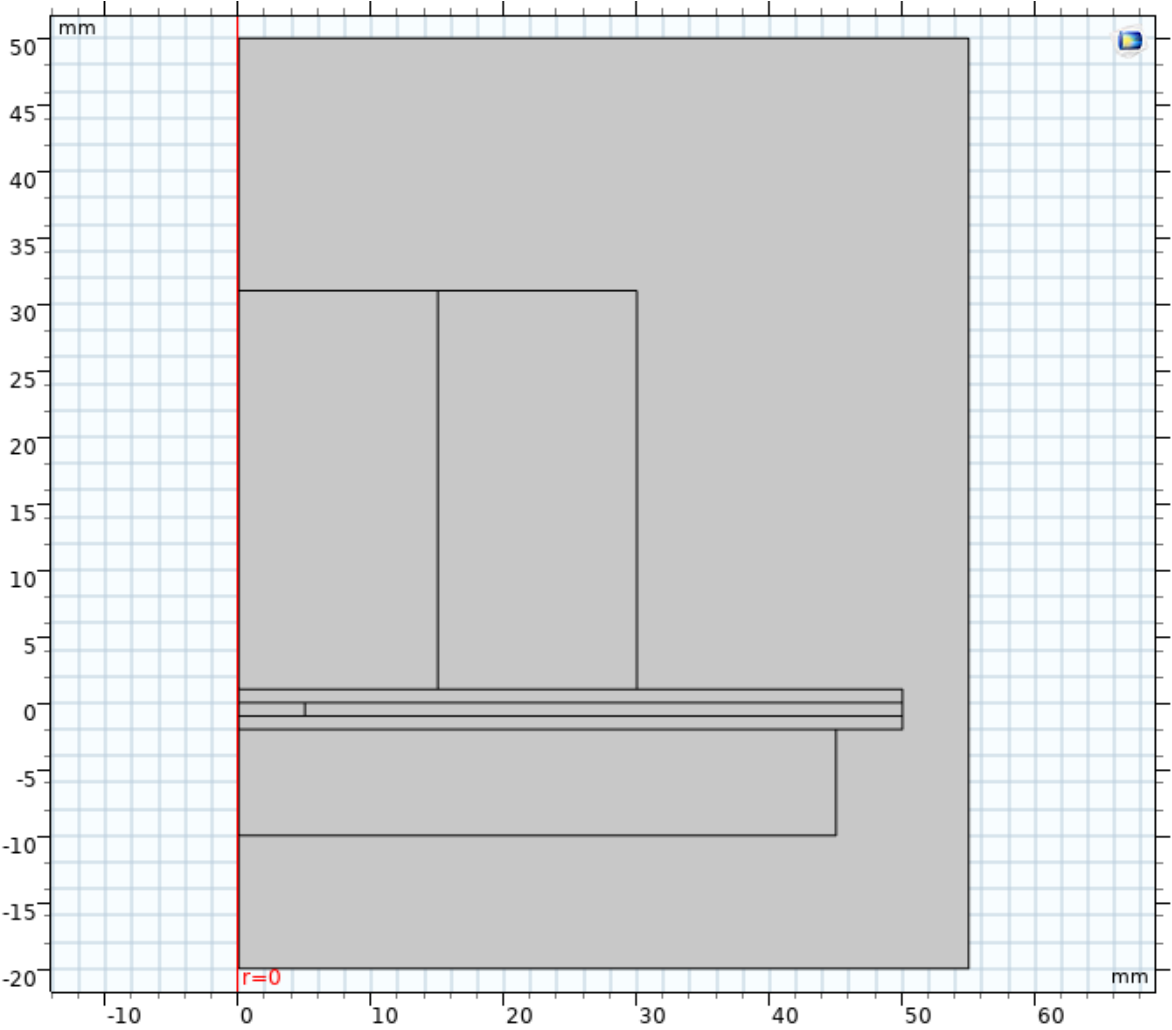
Figure 8: The model with a cylindrical void made with axis symmetry along y axis r=0. The void has a total diameter of 10mm in this figure.
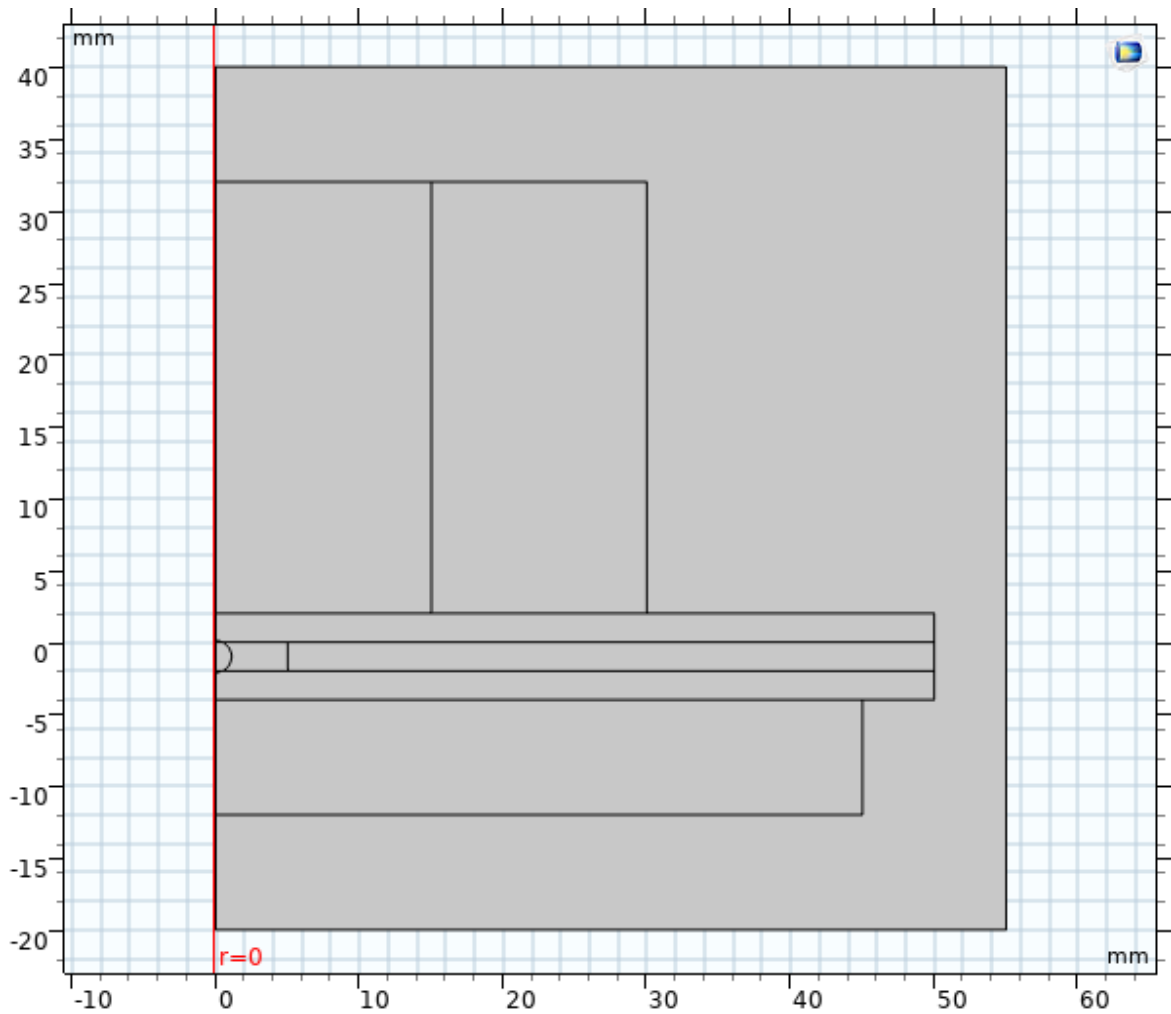
Figure 9: The model with a spherical void made with axis symmetry along y axis r=0. The void has a total diameter of 2.2mm in this figure.

3.1.2 Meshing

The model is meshed with "free triangular" in two different layers. The void within the insulation material is meshed with an extremely fine mesh with a maximum triangle shape of 0.06mm and minimum 0.0011mm. The rest of the model is meshed with the pre defined size called "normal". Here the maximum element size is 6.03mm and the minimum size is 0.027mm. The void has to be meshed with this small size in order for the electric field to appear as a smooth transition, hence making it easier to analyse the fields max, min and average fields. In Figure 10 the meshing of the model with a spherical cavity with a diameter of 1.2mm is shown.
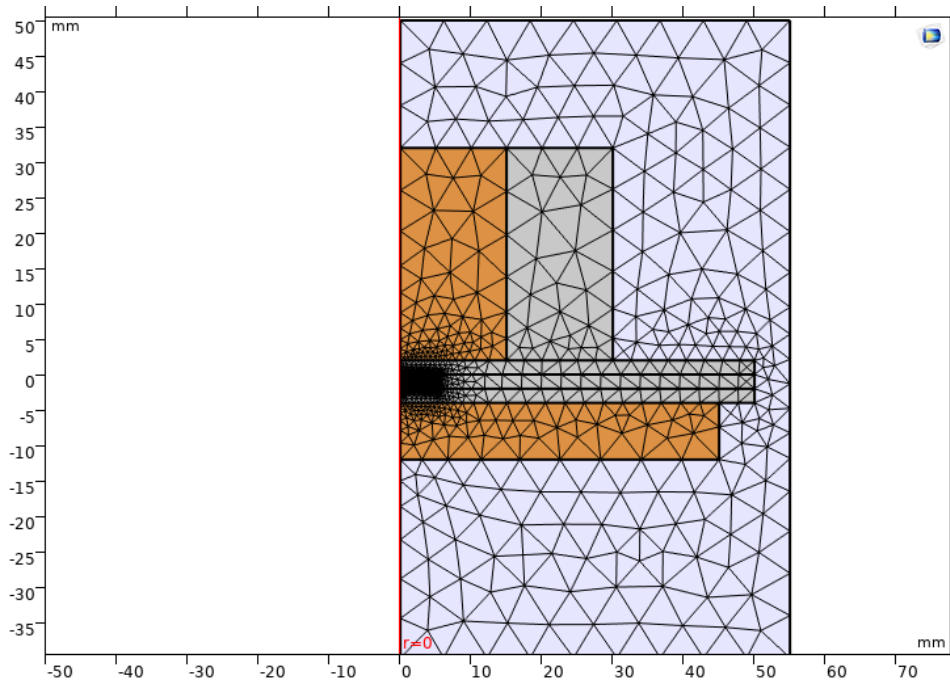
Figure 10: The meshing structure of the FEM-model. The extremely fined mesh in the void is close to solid black

3.1.3 Electric Field Measurement

The electric field for the cylindrical void have been analysed along two separate lines across the void. Figure 11 shows both area of which the field have been measured at, together with the point of maximum and minimum field. The plot is presented with a symmetry along y axis, so the presented length is equal to the void radius. Considering the change in void dimensions, the location of the line segments remain in a constant position for all tests.
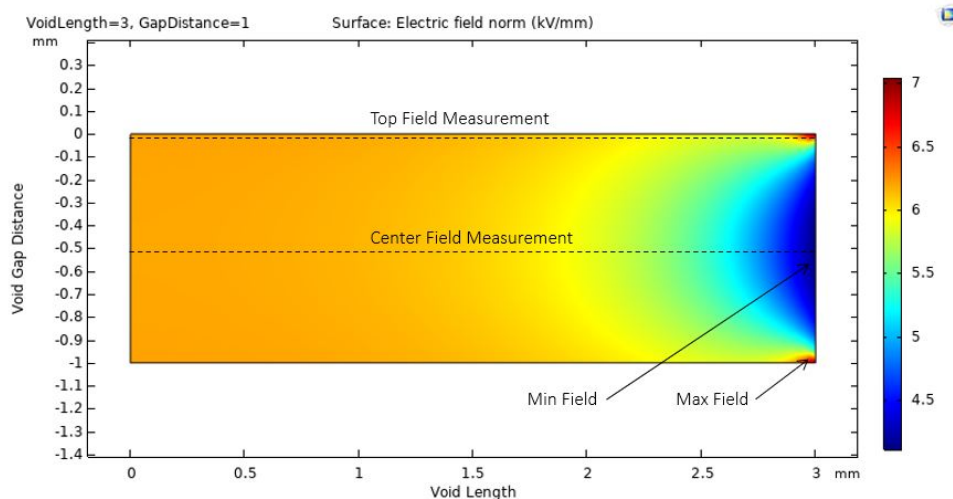
Figure 11: Illustration of the location of the measured points of the cylindrical void

15

3.2　Theoretical ABC-Model

The void dimensions from the FEM-analysis is adapted into a frequency dependent ABC-equivalent model. The void length is kept constant with an increasing gap distance from 0.2-2.2mm with a 0.4mm increase. The method for finding the inception voltage is described in the theory section by Equation 17 together with the Paschen law, Eq. 18. A pressure of 1 atm and a temperature of 20C(room temperature) is assumed.

Table 1: List of parameters used in the calculation of PDIV and apparent charge

| Parameter	Symbol	Value	Unit	Reference
Permittivity of insulation material	ϵ_r	3.4	1	[14]
Permitttivity of Vacuum	ϵ_0	$8.85{\cdot}10^-12$	Fm^{-1}	
Gap Distance	d	0.02-0.22	mm	
Insulation Thickness	D	$d{\cdot}2$	mm	
Mica/epoxy conductivity	σ_b	$2{\cdot}10^-16$	S/m	[14]
Air Conductivity	σ_c	0	S/m	[4]
Frequency	f	$10^{-5} - 10^2$	Hz	

3.3　Electrical Measuring Principle

The second part of this project is based on electrical detection of partial discharges in stator windings in hydro generators. The detection device used was from Omicron, and the measuring circuit is shown in Figure 12. A low pass filter was included in the circuit in order to sort out noise from the high voltage source. The coupling capacitor of 3.4nC is shown as Ck, and is connected to a coupling device, shown as the measuring impedance in the circuit. The capacitance provides for restoring of the voltage level during PD activity with current pulses. The quadripole measuring impedance, shown as CPL542 from Omicron, synchronizes the measuring equipment to the applied voltage. The PD signal from the test object is separated from the applied voltage with this impedance to the separated output of PD and V on the device. Another property of the impedance is that it may protect the data acquisition tool from dangerous and costly over-voltages and surges. The PD signals i processed in the data acquisition tools, which receives a voltage signal from the measuring impedance. The signal is processed through a fiber optic cable to the Omicron PD detection software through the control unit.

3.3.1　Test Objects

For this thesis four stator rods from a run-of-the-river hydropower station was analysed. Two rods which were service aged close to high voltage terminal, and two back-up rods which have never been in service. The rods came from "Øvre Fiskumfoss" power station in the northern part of Trøndelag County. The power plant was built in 1976 and it is assumed that the service aged rods have been in service for the last 43 years. The powerplant operates with a bulbturbine with a head of 54m and a total effect of 9MVA. The nominal voltage is documented as 3.2kV, and serves as the basis for the maximum voltage applied during lab testing. A testing voltage of U_{RMS}=1.8*U_0=3.3kV is applied during tests for all test objects.
All rods had a length to 1.6m, where both ends of 20cm where painted with field grading paint to prevent external PDs at the terminations.
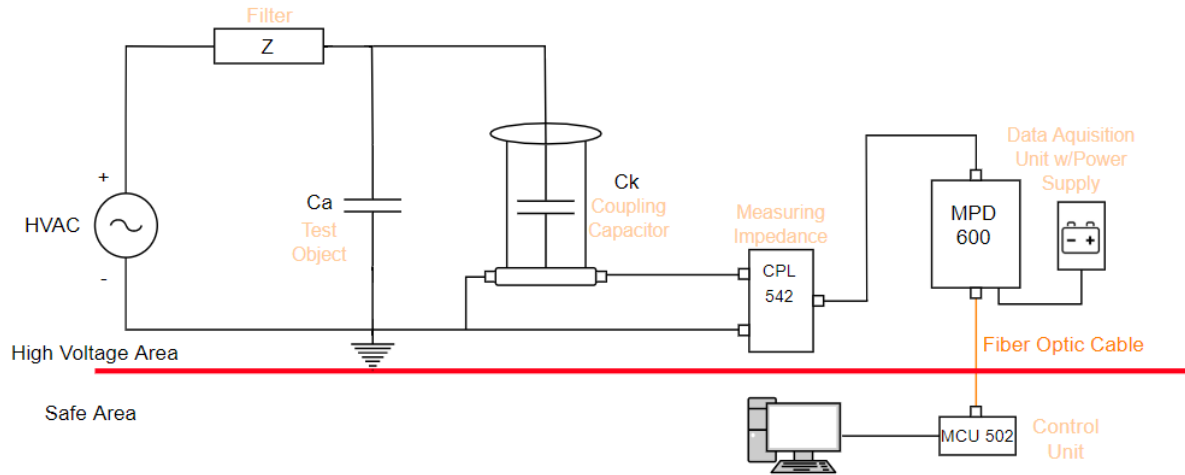
Figure 12: Test circuit used for the experimental electric measurement with OMICRON PD detection. The illustration was created for the specialization project by the author.

3.3.2 Calibration of Test Circuit

For each test object the circuit is calibrated in regards to both voltage and PD magnitude in order to obtain accurate results. Calibration of the voltage level was executed under high voltage while the charge calibration under zero voltage. When calibrating the circuit for charge, a known charge is injected over the test object, and the OMICRON software is then able to calculate a division actor between the coupling capacitor and the capacitances in the circuit. Voltage calibration is performed with a high voltage probe, measuring the voltage level on the high voltage side of the circuit. Again, the Omicron software is able to create a division factor in order to be able to analyse the exact voltage level the test object is exposed to with the software. Voltage calibration is only necessary to perform if the coupling capacitor or the coupling device is changed during testing.

3.3.3 Data Acquisition

When acquiring data from the PD activity in the test objects, the MPD600 partial discharge analysis system from Omicron are able to visualize and analyze real time PD detection and system parameters. The software allows us to record the measurements in real time so that we are able to run the entire test at a later occasion. This advantage gives us the possibility to study and repeat the details of the performed test like PDIV, PDEV and PD magnitude in a different location than the test facility. Omicron also facilitates for creating a data file containing this information to be exported in to a computational software like Matlab for further analysis. Test parameters obtained in thesis limits to PDIV/PDEV and charge magnitude.

Partial Discharge Inception and Extinction Voltage
These parameters are known as PDIV and PDEV, and indicates at what voltage level partial discharges occur and extinguishes in an object. PDIV is set after a repetition of discharges occurs with a minimal time delay, while PDEV is set for when the discharges no longer occurs under the limit of the detection threshold. The threshold in these test was set to 20pC. Because of the memory effect in insulation cavities, the PDEV is usually higher than PDIV.

PD Magnitude
The magnitude, coloumbs, of the partial discharges occurring, apparent charge q$_a$.

3.3.4 Voltage Controller and Test Programs

To control the voltage source during testing, a labVIEW program developed by Doctor Torstein Grav Aakre was used. Various voltage levels related to time or number of periods as well as the frequency level can be set before testing. Figure 13 shows how the voltage level was set for each test. Before testing a new test object, it was precondition for 5min at 50Hz for the maximum test voltage, 3300kV. This is in line with IEEE std.2014-34, Guide for PD measurement in AC electric machinery where a precondition test like this is suggested.

After preconditioning the same voltage increase and decrease is performed for 10 various frequencies ranging from 50Hz to 0.1Hz under 20C(room temperature) and 1atm.

The voltage is increasing in 10steps of 330V, where for each step the voltage is constant for 30s before it immediately increases. 30s is chosen as the voltage normally takes a few seconds to stabilize, in addition to not exposing the test objects to high voltage for a long period of time which can cause degradation.
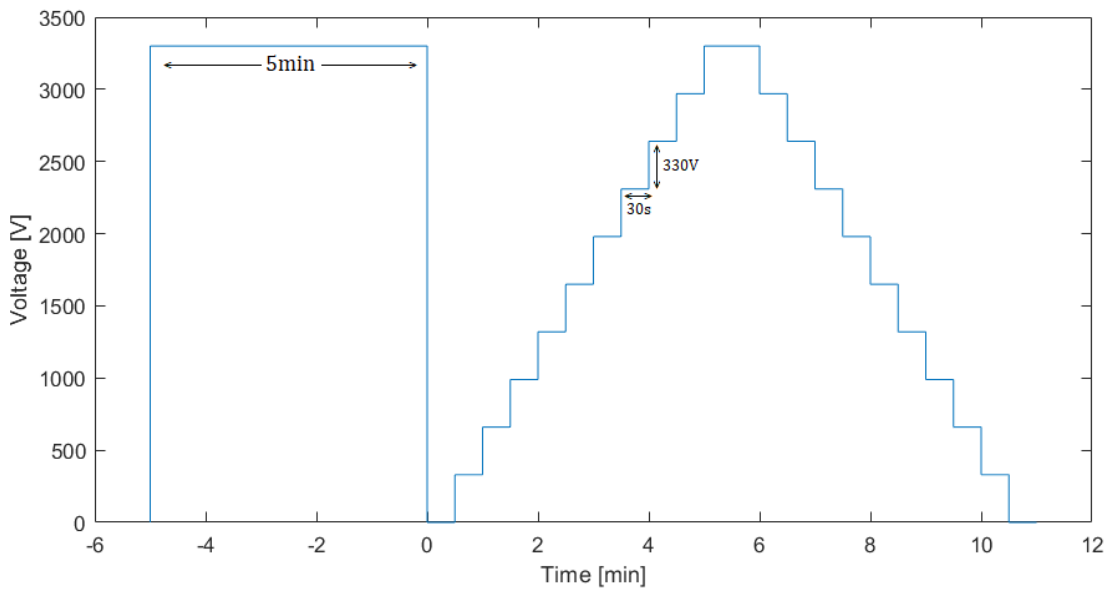

Figure 13: Voltage test control program used for the experimental tests on the generator rods. The steps increased with 330V for 10 steps until it reach the maximum voltage of 3.3kV.

4 Results and Discussions

4.1 FEM Analysis of the Electric-Field in Air-Filled Voids

This section will highlight the impact various geometric dimensions of voids has for the electric field and the edge effects. Using numerical simulations in a FEM tool, a realistic picture of how the electric field will change in a void related to its dimensions. By studying the electric field, the relationship between the field and the PDIV can be analysed.

4.1.1 Cylindrical Void Geometry

The cylindrical void is modelled with a diameter range from 2mm to 20mm, with the gap distance varied from 0.2mm to 2.4mm. This means the voids geometries is varying between short and wide, and tall and narrow cylinders. It is known that the electric field is more homogeneous when a void has a large area with small gap distance. When looking at the plots it is expected that the field will be close to homogeneous as the diameter increases with a fixed gap distance. The electric field at the corners are higher than anywhere else in the void. Taken in consideration the edge effect, the field is measured both along the top edge and through the middle of the void.

The following figures represents the visual of how the air voids are modelled. Figure 14 shows a tall and narrow cylinder, often caused by cracks in the insulation material, while the wide and short cylinder is often caused by delamination. In comparison it is evidently that there are more inconsistencies in the electrical fields in the tall and narrow cylinder, by the judge of the color scheme presenting the electric field.
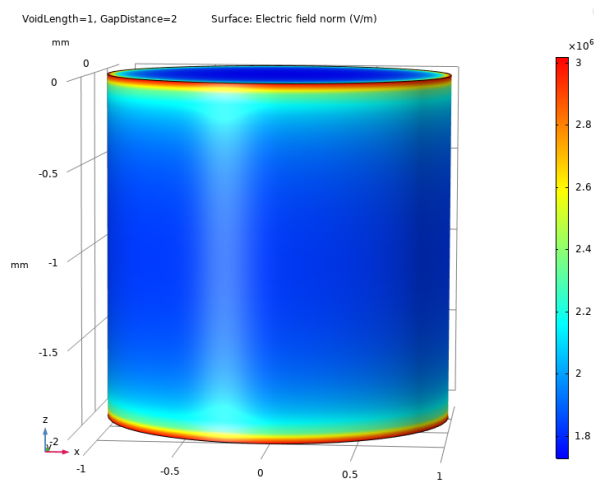

Figure 14: Air filled void with a diameter of 2mm and gap distance 2mm visualised by electric field distribution.
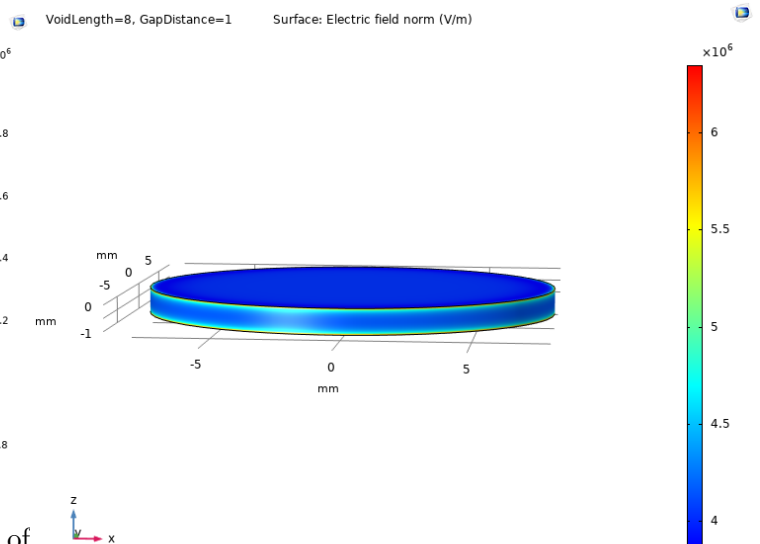
Figure 15: Diameter of 16mm and gap distance 1mm.

From the 3D revolved geometries of the void, we can see that it appears to be true that the electric field is stronger along the top and bottom edge of the void.

Electrical Field in Cross Section of Voids

The plots given in the figure below show the electric field distribution with a fixed gap distance of 1mm, for three various gap lengths. A constant voltage of $\sqrt{2} \cdot 7$kV is applied.
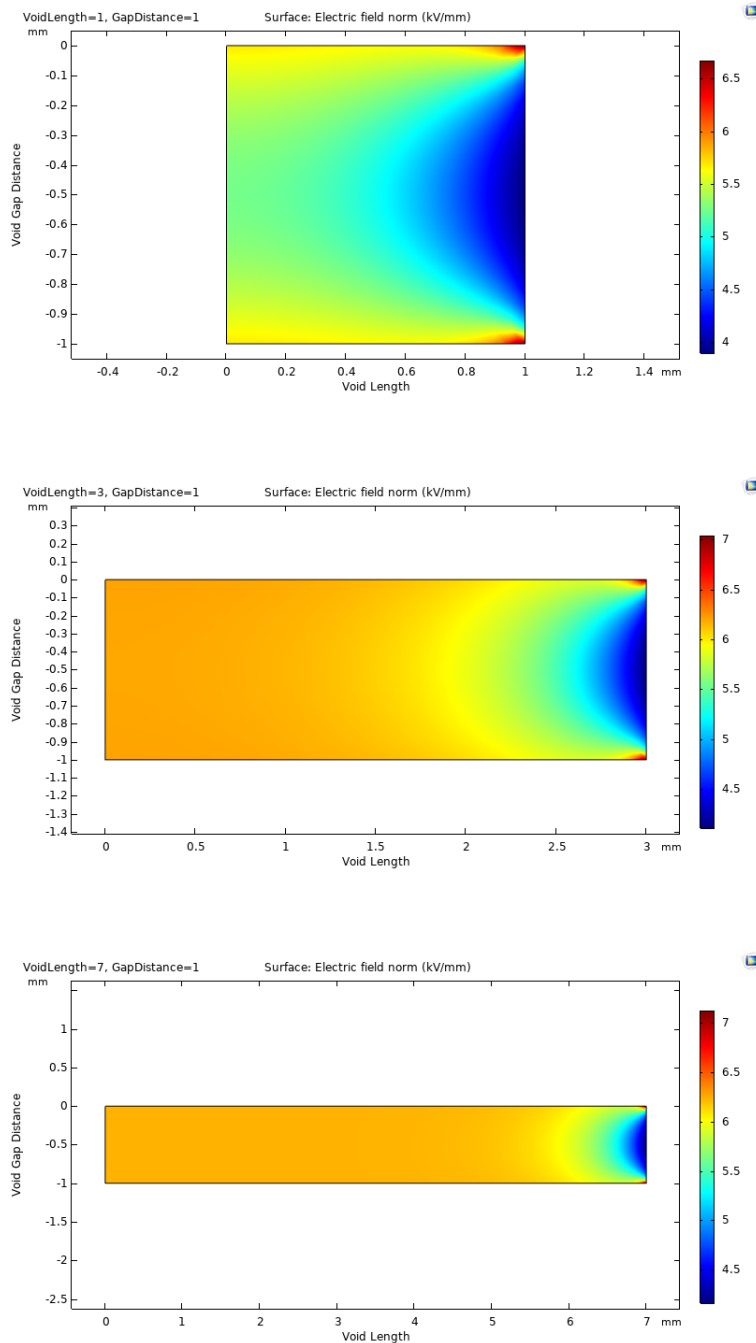
Figure 16: The electric field distribution of a cylindrical void with fixed gap distance=1mm with increasing void length. Symmetry along y-axis.

Looking at these distributions, the field is not homogeneous in any of the plots. However, the field becomes more homogeneous as the area expands. The weakest field, colored blue, is found at the center-end of the void, and there is minimal change in the extent for this area for all void lengths. The overall field strength is increasing along with the diameter. In Figure 17 the electric field as a line distribution along the middle and outer fields is shown. As the void diameter increase, also the field enhancement is increasing. The

biggest increase is happening from 2mm, where the average field strength is increasing with about 15% from 2mm to 6mm. When increasing from 6mm to 10mm, the same effect only is increased with close to 2%. This indicates that the field is dependent on the relation between the void diameter and the gap distance.

From Figure 16 we can see that the corner effect is easily visible, and the field is substantially higher than any other part of the void. Studying the line diagram, it is also clear that the field in the corners increase with increased void length. This increase is also greater within the lower lengths, and this increase seems to decline as the void length increases.

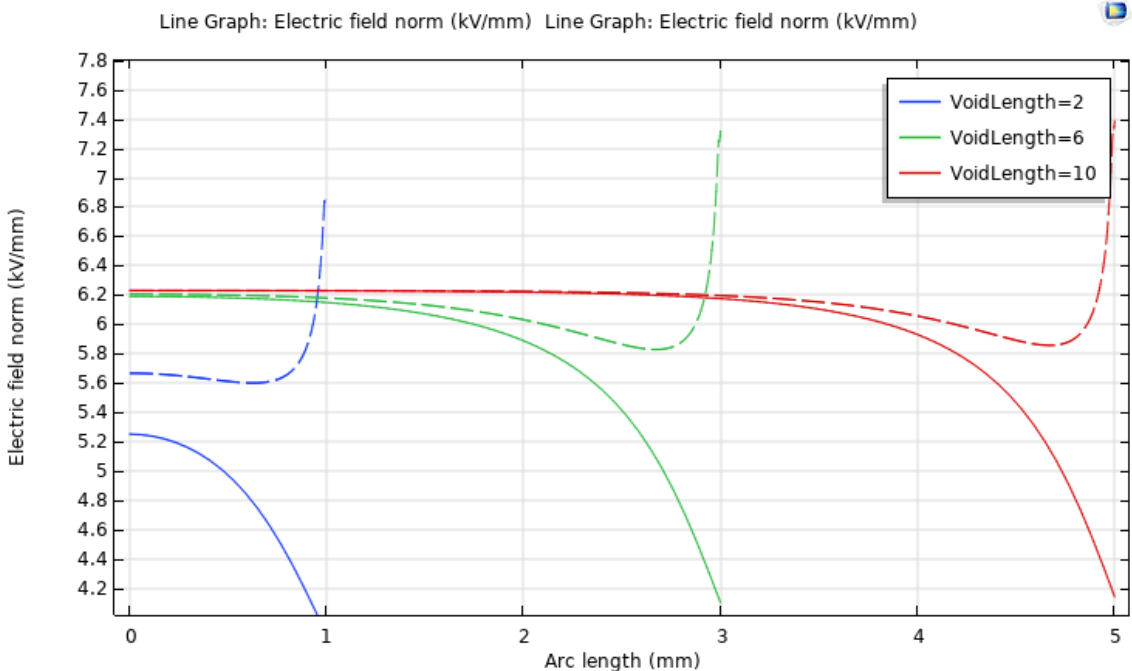
Figure 17: Electric field distribution along two lines of an air filled void with fixed gapdistance of 1mm. Solid line equals the field running along the center of the void, while stapled lines represents the field along the very top of the void.

Choosing to study the void with a length of 2mm with a variable gap distance, we can analyse of the field is changing in terms of change in areal. We know that the electric field tends to be more homogeneous with a small gap distance but large area, and thus it is interesting to see just what dimensions are right for this claim.

Figure 18 shows how the electric field changes for a 2mm void in relation to a gap distance varying from 0.2-2.2mm. When the gap distance has reached its highest value of 2.2mm, making the cylinder taller than its wide, is when the biggest change in electrical field distribution occurs. The field throughout the center of the void decreases minimal, while we can see that at the top the field appears to differ a lot from the center, as well as the corner effect is the greatest at this gap distance.
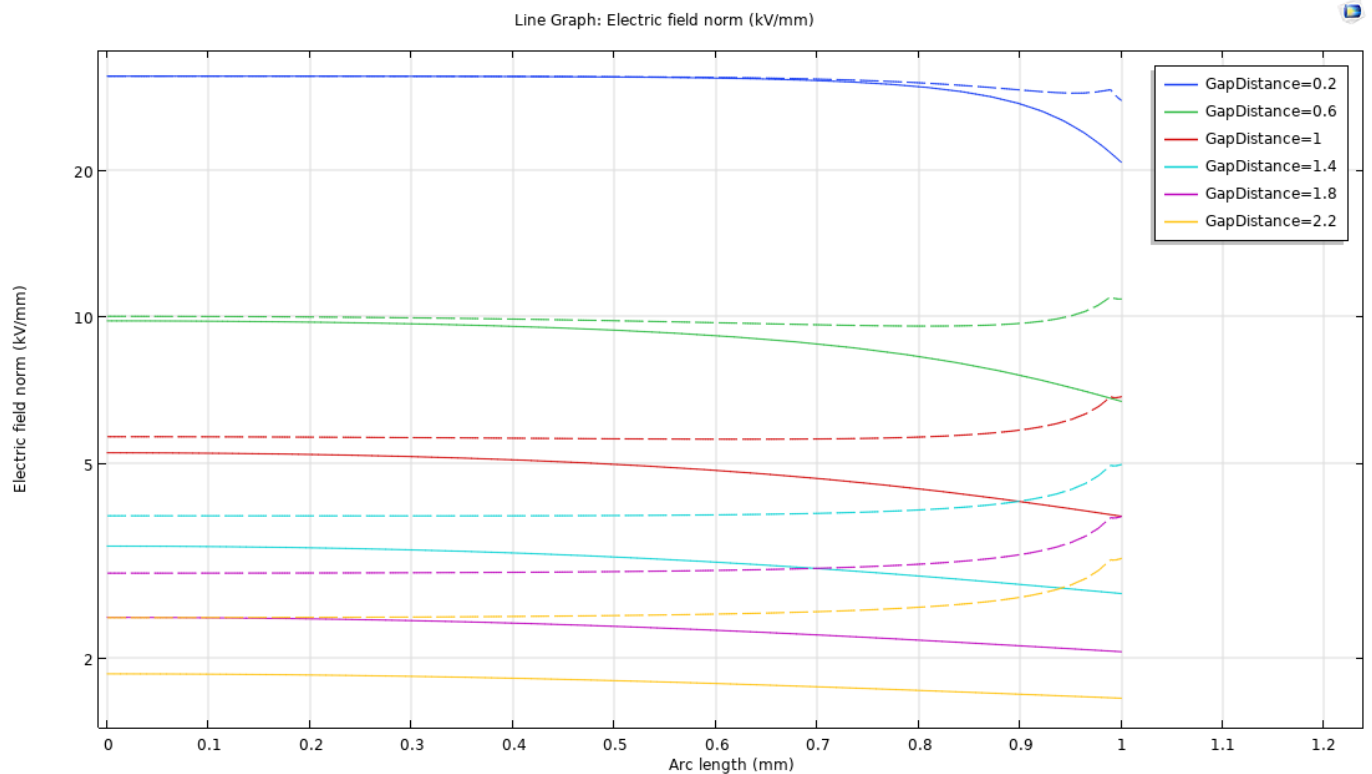

Figure 18: Electric field distribution in a 2mm void with various gap distances for both top and center line of the void.Solid line equals the field running along the center of the void, while stapled lines represents the field along the very top of the void

As expected, the field is at its most homogeneous when the gapdistance is at its smallest, 0.2mm. Even though this is considered close to homogeneous, the field in the center decreases with 32% from its highest field at 31kV/mm to 21kV/mm at the end of the center, colored blue. What is interesting about this dimension, is that the edge effect seems to not follow the trend of increasing field value like for the other gap distances. For the dotted line showing the field in the very top, the field is decreasing by a very small amount at the very end.

Looking at the 2D plot for this dimension in Figure 19 we can see the visualisation of this distribution throughout the gap.

When the void length is 10x larger than the gapdistance as this this case is illustrating, there is no clear presence of the edge effect. At the very corner of the gap the low electric field from the middle end is exceeding in size than the high homogeneous field in the rest of the void, cause a very small to no drop in voltage show in Figure 18.
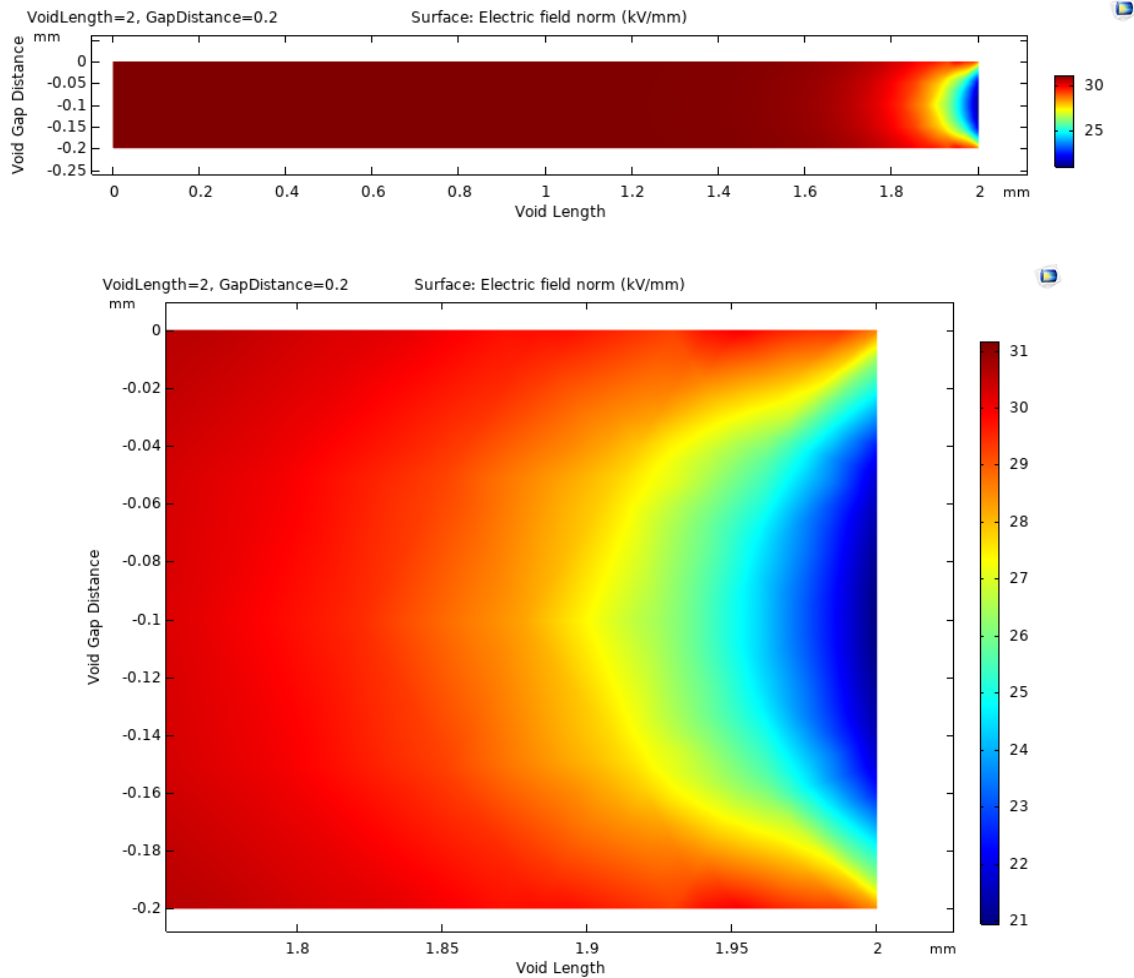
22

Figure 19: Electric field field distribution in a 2mm Void with gap distance= 0.2mm

In Figure 19 the field is equal to homogeneous throughout its lengths. From 1.85mm the change in the electric field starts to decrease. The magnitude of the field decreases to its minimal value at 2mm, about 21kV/mm. This yields a field enhancement f of 2.1. This is equal to the electric stress on the rest of the insulation surrounding the air gap. The maximum field, about 31kV/mm is found in the middle of the void. This yield a field enhancement of 3.1, very close to the theoretical enhancement of ϵ =3.4.

4.1.2 Edge Effect

We have seen that the edge effect is stronger when the relation between the length and gap distance is increasing. At a certain length-gap ratio this effect seems to decrease, but for each length the ratio varies. In Figure 20 the electric field distribution for a gap distance of 0.2,0.4 and 0.6mm is shown for various lengths of the void. Commonly for all dimensions is that the field is close to homogeneous with the exception of the edge effects. The gap distance of 0.2mm have the smallest area when the void length is 2mm, and the edge effect is not present at this ratio where the gap distance is 10% of its length and an area of 0.4mm. For the 0.4mm gap distance, it is clear that for all lengths the edge effect is present, even when it achieves the highest area of 8mm where the gap distance is only 2% of its length. For 0.6mm gap distance the edge effect occurs also for every void length.

The magnitude and area of where the edge effect occurs slightly increases as the area of the voids decreases. However when the area increases, the electric field at the very corner of the void, is bigger than for lower areas.

The biggest change in the area affected by the edge effect is easily visible for the 0.6mm gap distance, as the curve of the electric field at 1mm is to a slight extent larger than for the other lengths.
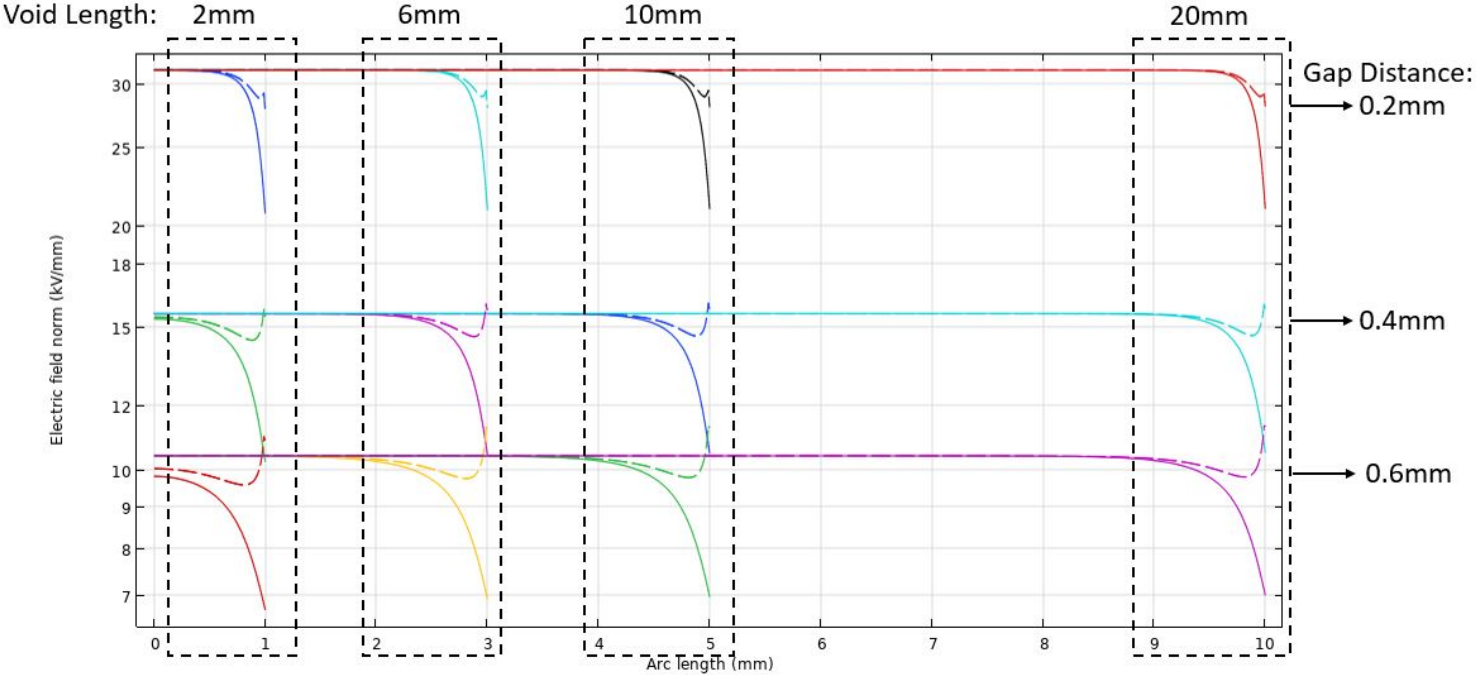

Figure 20: The electric field strength for the lowest gap distances used in this test with a variety of void lengths in order to study the edge effect behavior.

4.1.3 Spherical Void Geometry

For a spherical cavity it is assumed that the electric field will be homogeneous as long as the spherical diameter is not close to the total thickness of the insulation material [15]. The theoretical electric field is found by Eq. 7 and compared to the simulated void in the FEM tool. A voltage of $\sqrt{2}\cdot7$kV is applied to the model.

The electric field in an air-filled void with a diameter of 1/3 of the total insulation thickness is given in Figure 21 .

The results shows that for void with diameter under 10mm the simulated electric field is equal to the theoretical. A small offset of 24% from the theoretical value occurs at 10mm. The biggest void-diameter tested was 10mm yielding a total insulation thickness of 30mm, the same length as the HV conductor in the FEM-model. The inconsistency for the electric field at 10mm can thus be seen in relation to this dimension conflict.

Although, it can also indicate the theoretical field is more accurate for voids under 10mm.
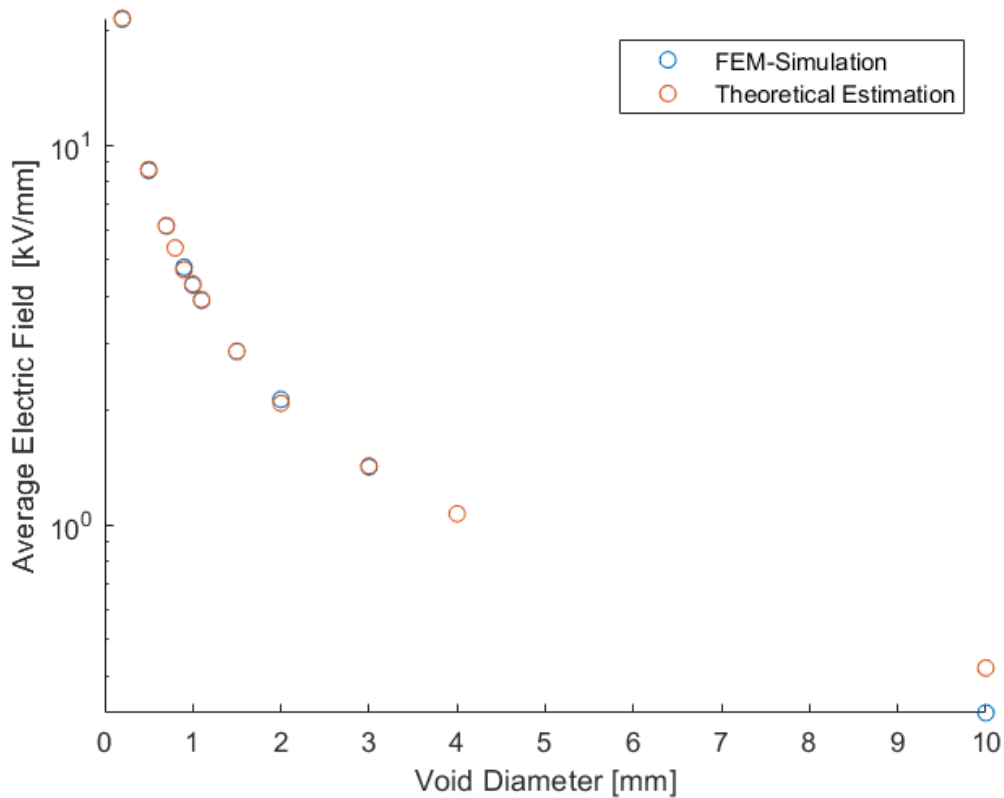

Figure 21: Comparison of the average electric field in a spherical cavity with varying diameter, from FEM analysis and theoretical analysis

Fixed Insulation Thickness

To understand the change of electric field when the void diameter increases more than 1/3 of the insulation thickness, a comparison of the electric field with an increasing void diameter to insulation thickness ratio is evaluated.

In Figure 22 the solid blue line represents the theoretical maximum electric field when the insulation thickness is at 2mm in three layers with no cavity present. Because of the insulation thickness does not increase in this test, the electric field remained constant for the length of the HV conductor, 15mm, and throughout the thickness of the insulation. As the diameter of the void never exceeded 10mm, the field is assumed homogeneous when no voids are present.

The smallest void diameter tested at 1.1mm is already exceeding one insulation layer by 0.5mm on top and bottom, compared to a void of 1mm where the sphere void is placed right inside one layer. With this change in dimension, knowing the void now exceeds the 1/3 insulation thickness limit we can tell from Figure 22 that the average electric field is lower than from the theoretical analysis. As the voids diameter continues to increase, reaching closer to having the same thickness as the total insulation, the average electric field decreases by 70% from the theoretical value.
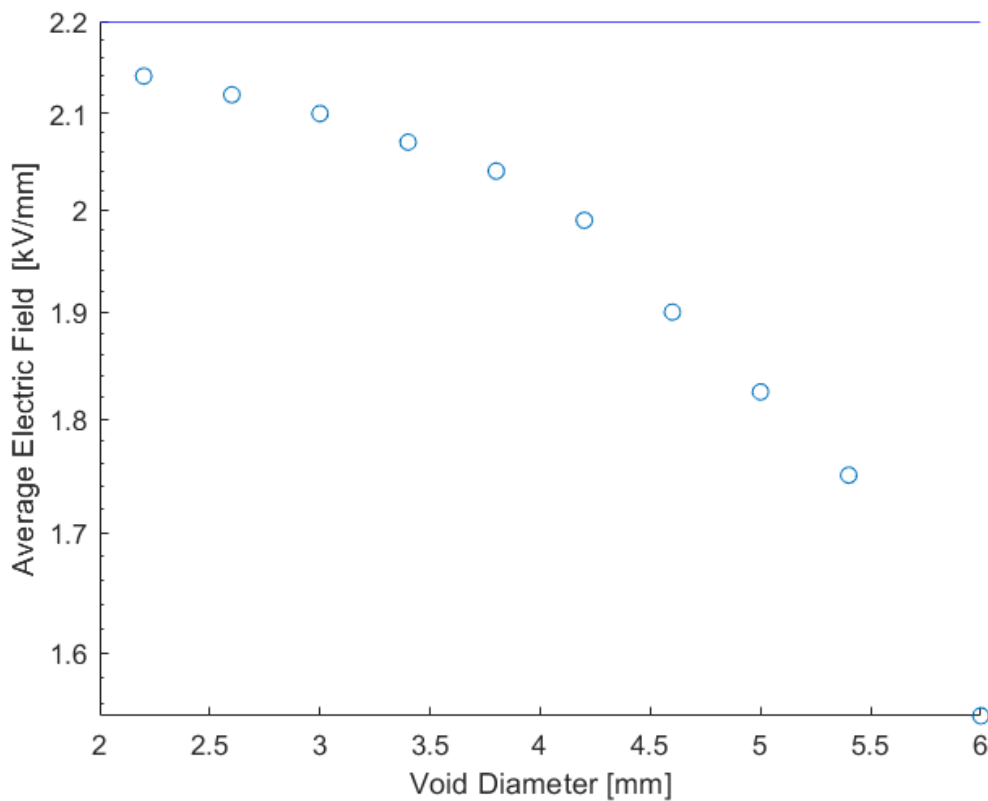
Figure 22: The average electric field in a spherical void with increasing diameter with a constant insulation thickness of 2mm.

Figure 23 shows the maximum, average and minimum electric field strength in the spherical void as a function of the void diameter. With increasing void diameter, the maximum field is decreasing.

From 1mm to 3mm the max. field decreases by 7%. For the min. field in the void, the electric field decreases by 40% from 1mm to 3mm. However, the area of the max.field appears to be greater than the min. field for all diameters as the average field is in close relation to the max. field. This indicates that when the void diameter is equal to the insulation length the field is strongly affected by the distance to the ground electrode as the min. field is very low, yet the average field only yields a 13% field drop from 2mm to 6mm.

Figure 23: Maximum, average and minimum electric field strength in a spherical void with increasing diameter.

4.2 Modeling of Frequency Dependency: ABC-model

4.2.1 PDIV Estimation

The estimation of the theoretical PDIV of a void can be found with the expression given in Equation 17 together with the breakdown voltage fro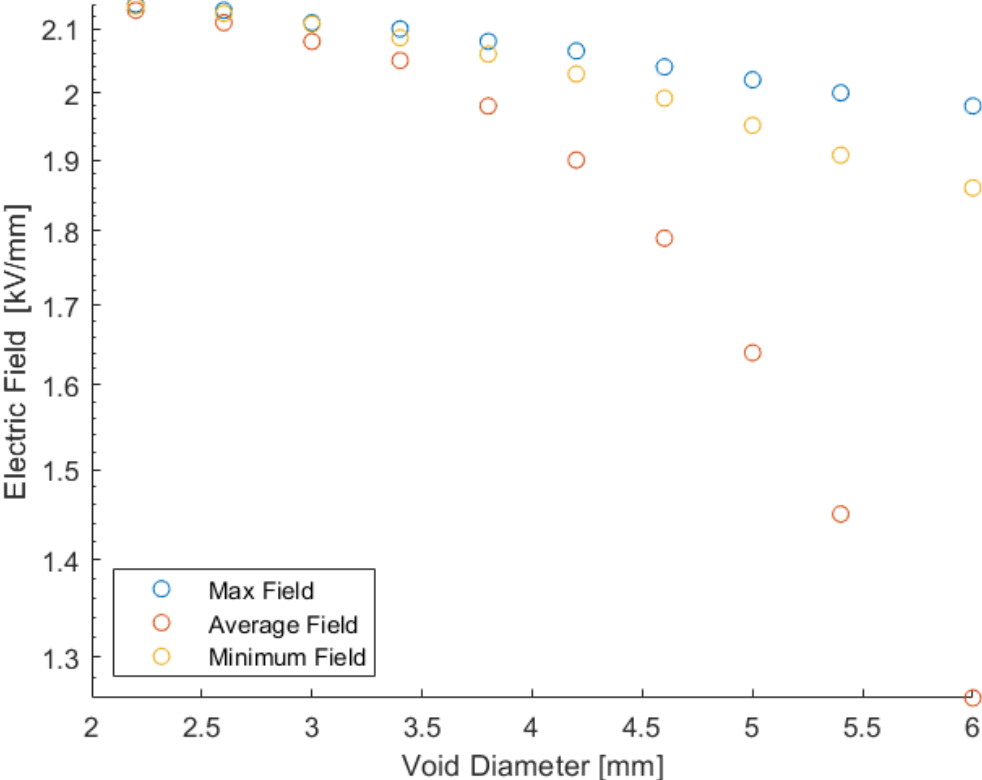m the Paschen curve in Equation 18. The breakdown voltage, U_s, for all gap distances is found with the Paschen curve in Equation 18 and presented in the following table.

Table 2: The breakdown voltage, U_{s0}, found for a range of gap distances under atmospheric pressure with Equation 18.

Gap Distance [mm]	U_s [kV]
0.2	1016
0.6	2197
1	3225
1.4	4189
1.8	5116
2.2	6018

The frequency dependent model includes along with the Paschen curve for breakdown value, a combination of permittivity and conductivity, thus creating a frequency dependence of the PDIV simulation. The conductivity of the insulation material, σ_b, is chosen based on a study under nominal temperature, 20C. From the FEM-analysis we know that the electric field increases with decreasing gap distance of a cylindrical void. It is expected to observe a smaller PDIV for the smallest gap distances because of the relationship with the electric field and the breakdown voltage.

By using the same void gap dimensions as in the FEM-analysis in Figure 18 in a frequency dependency study, we are able to see the impact of frequency on the inception voltage. The results of the PDIV analysis is presented in Figure 24 and shows that the PDIV level increases along with the increase of gap distances as expected. The PDIV level seems to have a close to linear increase from the shortest to the longest gap distance.

In the VLF range the PDIV is decreasing as the gap distance is increasing. For the smallest distances the PDIV is close to unaffected by the frequency level, while there is a bigger difference for the larger gapdistances in the VLF range. For the 0.2mm gap distance there is a 4% change between the highest and lowest PDIV found. For the 2.2mm there is a 16% decrease in the PDIV between the highest and lowest PDIV found. For the low frequencies the PDIV is more affected by the conductivity, and for the higher frequencies the permittivity is influencing the PDIV.
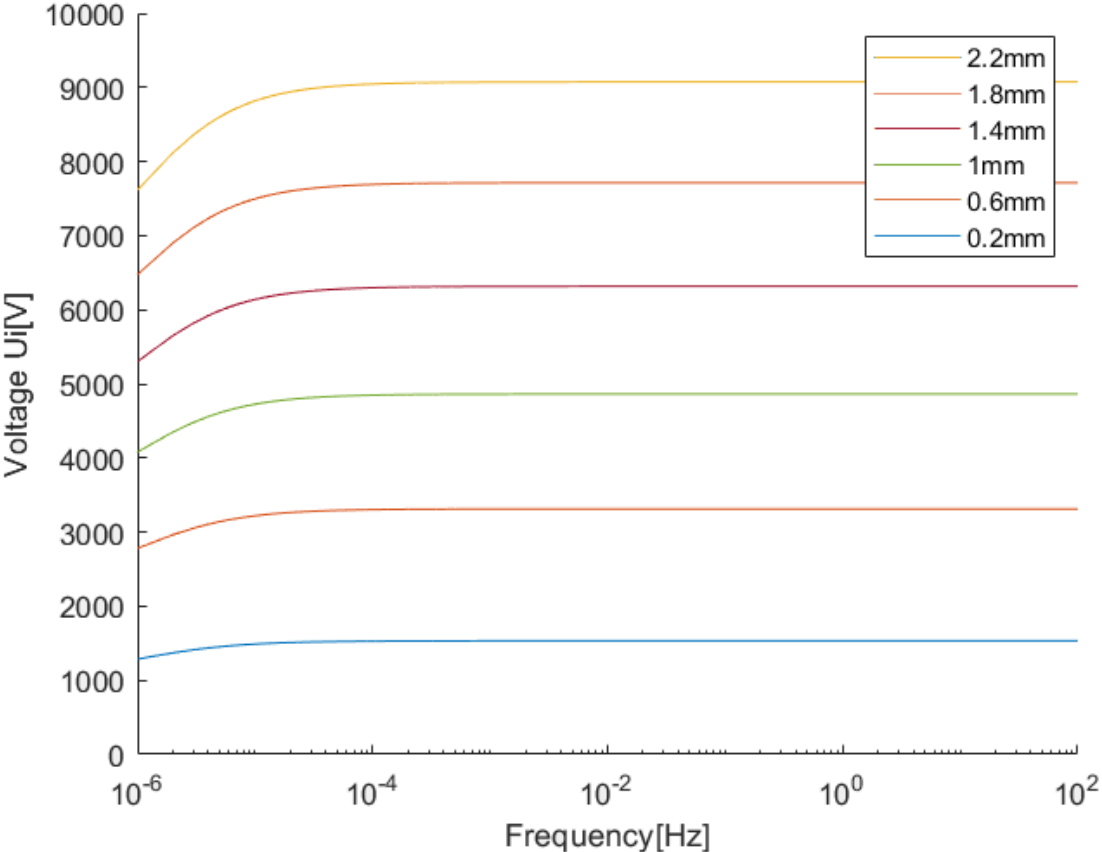
Figure 24: PDIV of voids with a gap distance varying from 0.2-2.2mm

4.2.2 Apparent Charge Estimation

The theoretical apparent charge is found by the relation of the capacitive abc model given in Equation 11 and the Paschen law given in Equation 18. The atmospheric pressure within the cavity in assumed to be equal to atmospheric pressure. Because the characteristics of the discharges is not studied, the remanent voltage is assumed negligible and the lowest voltage level of breakdown is considered as U_{s0}. The void electrode area chosen based on a gap length of 2mm, so the total area will is equal to $\pi \cdot 10^{-3}$. The total thickness of the insulation is increasing 3 times the gap distance for each test.

Table 3: The maximum apparent charge for the various gap distances with void length=1mm

Gap Distance [mm]	Max. Apparent Charge [pQ]
0.2	240
0.6	173
1	152
1.4	141
1.8	134
2.2	129

Figure 25: Maximum apparent charge curve for a cylindrical void with varying gap distance under 1atm.

4.3 Electrical Measurement of Laboratory Objects
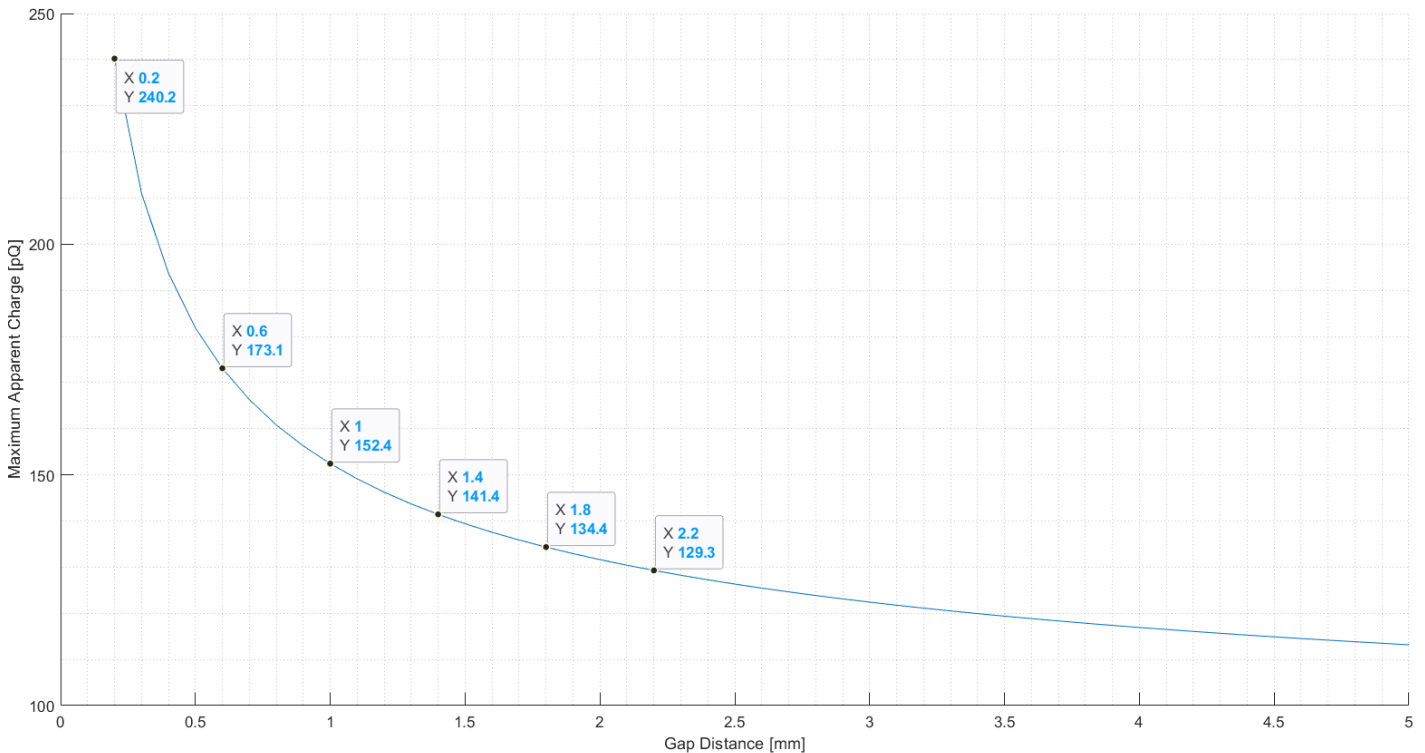
The PDIV and PDEV plots of service-aged and back-up generator rods are presented in the following plots. As the back-up rods are intended as critical spareparts for the stator, it is favorable to that the condition of these rods are in the same condition as new rods are supposed to be. All rods have been applied a voltage of 3.3kV RMS under room temperature, 20C.

4.3.1 PD Inception and Extinction Voltage

The results for PDIV and PDEV for the back-up rods tested is presented in Figure 26 and 27. It shows that the variation between the PDIV and PDEV levels at all frequencies are very low. As there is no clear trend between high and low frequencies, the PD activity is not dependent of the frequency chosen in this tests like proven in Section 4.2.

In Figure 26 the largest variation present for PDIV is a 12% increase from 50Hz to 10Hz and a 20% increase in PDEV from 40Hz to 0.2Hz. However, as the voltage was applied in steps of approximately 330V the very exact moment is hard to decide. This factor along with the rods are only designed for a nominal voltage of 3.2kV this can affect the PDIV and PDIV by +-10%, making the variation more insignificant.

The condition of the two back-up rods can be considered equal by the means of the results from the PDIV and PDEV analysis, as the results from both rods is comparable with no significant difference present.
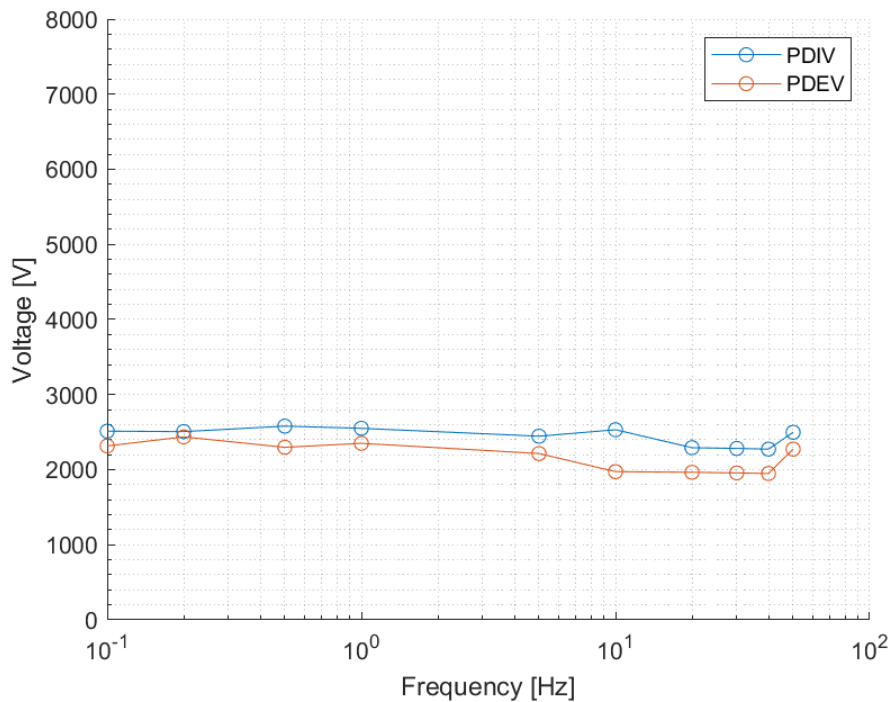

Figure 26: PDIV and PDEV collected from a non-serviced generator rod labeled R1 .

31
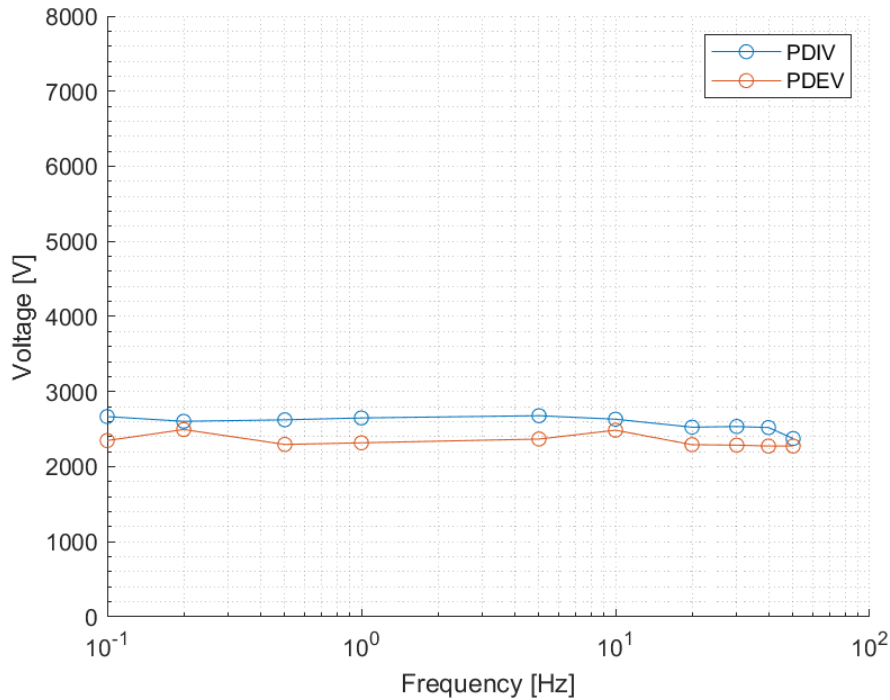
Figure 27: PDIV and PDEV collected from a non-serviced generator rod labeled R2 .

The PDIV and PDEV plots from the two service aged rods are presented in the following plots. Also here the frequency dependency is insignificant for both test objects as there is no clear deviations.

In comparison, the second rod, S2, shows that PDIV and PDEV occurs on a lower level than for the first rod. The average PDIV level is 50% lower in the second rod and the average PDEV increased by 48%. This is an indication that the condition of this rod has decreased during service as it is assumed that all rods were in the same condition originally. The nominal voltage of the operating generator is given as 3.3kV, meaning that the generator rods are exposed to a voltage of approximately 1.8kV under operating conditions. The average PDIV of service rod S2 is 1.3kV, which is 500V under the operating voltage. Operating the generator with stator rods in this condition can be cause harmful and costly failures to the machine if not corrected.

For service rod S1, the PDIV and PDEV is equivalent to the condition of the back-up rods. The average PDIV is 2.6kV for this rod, well above the operating voltage of the generator.
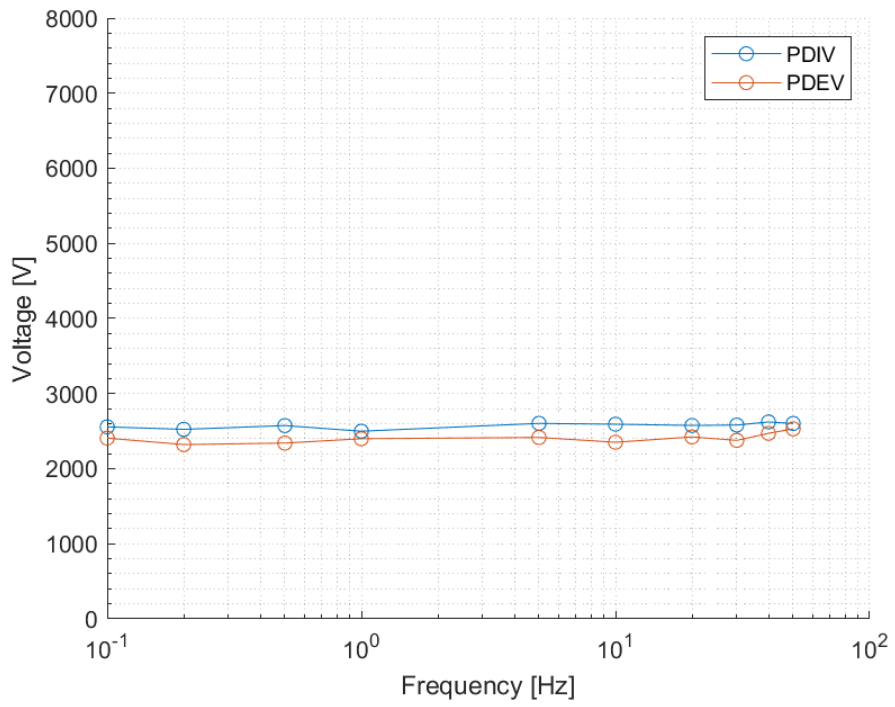
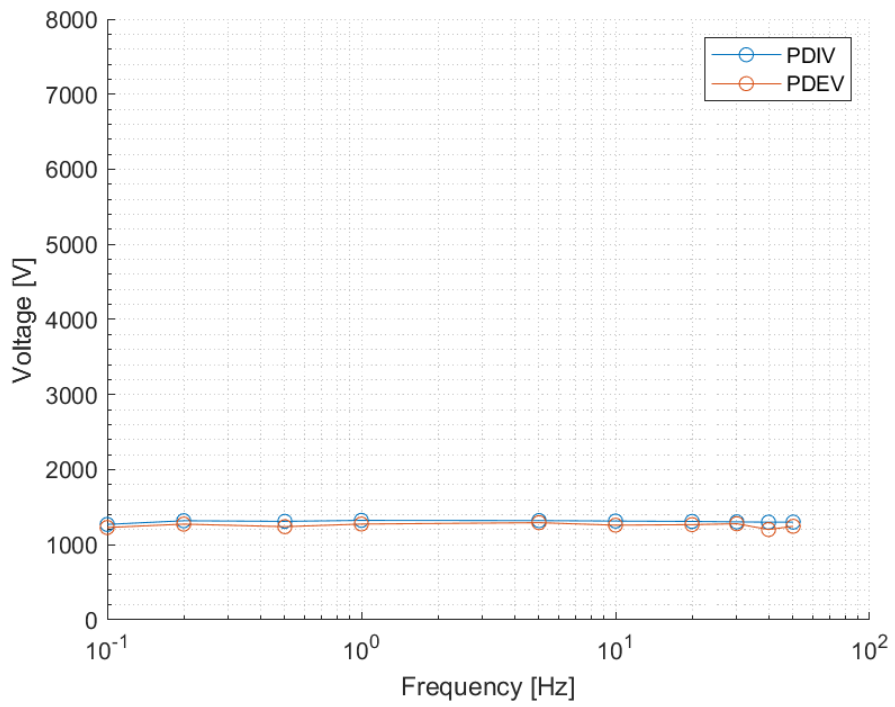Figure 28: PDIV and PDEV collected from a service aged rod, labeled S1 .

Figure 29: PDIV and PDEV collected from a service aged rod, labeled S2

By the physical looks of rod S2, seen in Figure 30, it was evident that they have been restored to some extent. This could be seen at the outer diamonds coils when the insulation was removed. The strand insulation had severe delamination and air voids along the conductors. Also in the cross section of the removed insulation some delamination was present inside the rod groundwall insulation. However, it is difficult to see how deep these air voids go inside the insulation, or if they have occurred due to the physical removal of the insulation for this testing purpose. For all four rods tested this was the only rod with this characteristics.

It is imaginable that these voids have occurred during repair of the voids, as the copper conductors was also found slightly crooked and it appeared in the diamond connection between the rods. As the voids are appearing in parts of the rod surrounded by field grading paint, there is a low electric field in this area, thus it is unclear how this affects the resulting PD inception and extinction levels.

Because of the rough characteristics for this part of the rod, it may be translatable to the operating conditions for the machine and to the rest of the rod insulation with a higher electric field. By removing this part of the rod it would be possible to observe if this part have any affect of the resulting inception voltage.
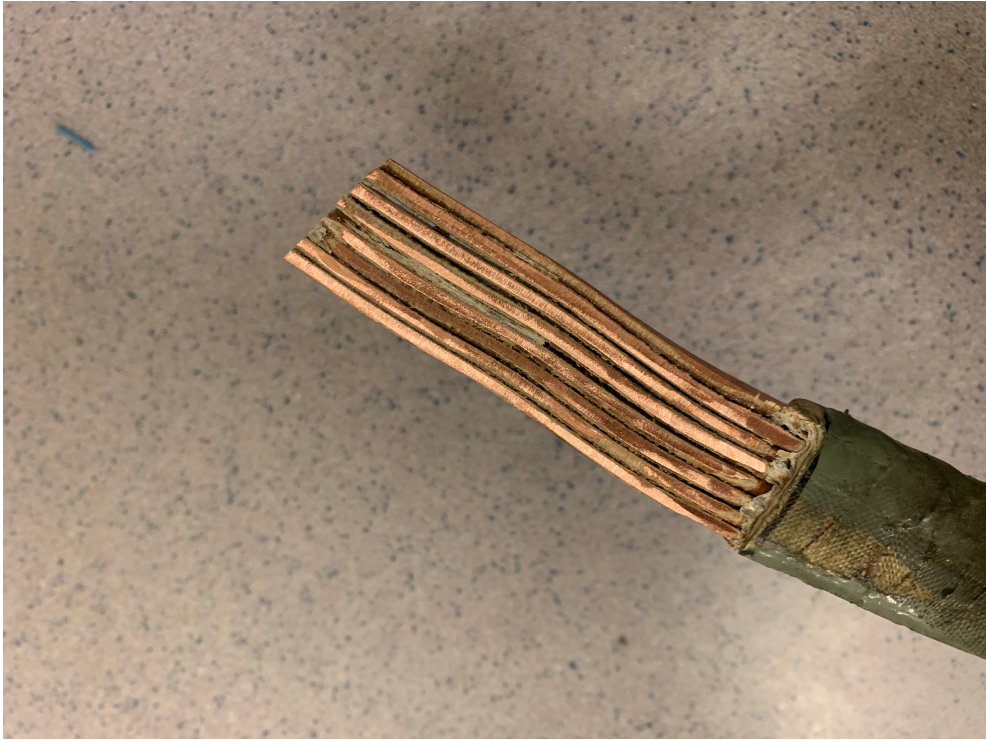
Figure 30: Stator rod S2 where the insulation of the end of its diamond connection is removed.

4.3.2   PDIV Void Distance Estimation - ABC-model

When knowing that the PDIV of the service aged rod(S2) is 1300kV, the ABC-model can be used to estimate what void size is contributing to the occurrence of PDs, Eq. 17. Assuming a relative permittivity, ϵ_r, of mica/epoxy to 4 [12]. The total thickness of the rod is 1.5cm, and σ_b is set to $2 \cdot 10^{-16}$. The PDIV was frequency independent, and set to 50Hz in the frequency dependent ABC-model.

With these parameters the theoretical PDIV plot shows no correlation to the experimentally measured PDIV. The lowest PDIV found in the theoretical model was 2920kV with a void with distance 1.9mm. This value however is closer to the PDIV found for the 3 other rod samples. This can indicate that there are other factors contributing to the PDs occurring at this low voltage level, like surface discharges. The choice of parameter constants is also a source of error, as the exact relative permittivity for these rods is not found along with the measurement of the total insulation thickness may have marginal errors.
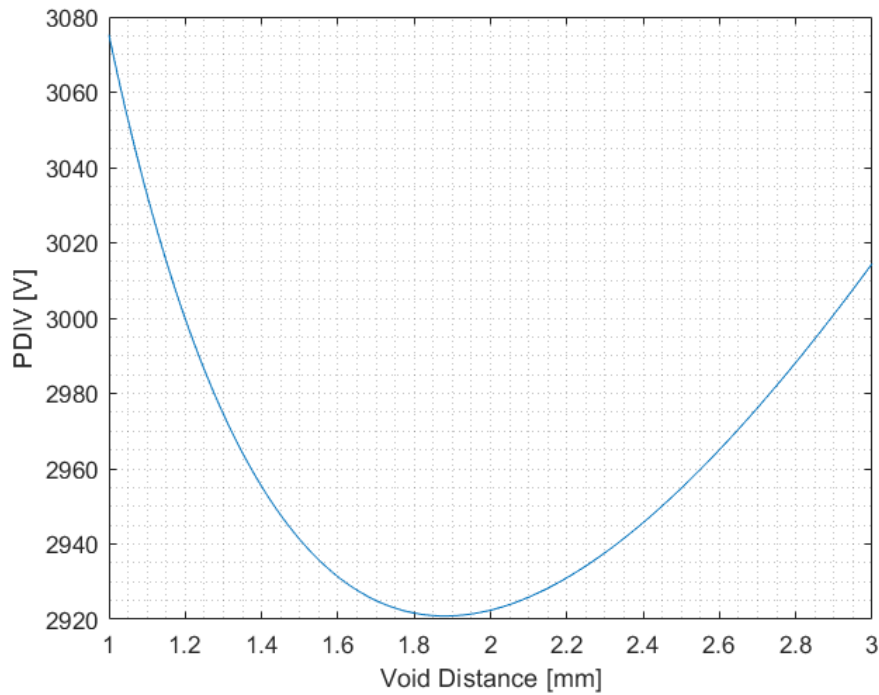
Figure 31: PDIV to gap distance relation for the experimental test objects

4.3.3 Charge Magnitude

The average charge magnitude was collected for back-up rod, R1, and the service stressed rod, S2, and compared in Figure 32. Because of the low PDIV in the service stressed rod, it was expected that the charge magnitude was higher than for the back-up rod. As PDs started occurring at 1.3kV, while the peak voltage during testing was set to 3.3kV both the number and magnitude of the PDs are able to increase in size for a longer period of time under stress. At 50Hz the difference between the rods shows an increase of the average charge magnitude of 87%, while for 0.1Hz there is a difference of 92%, meaning that the charge for both rods is equally frequency dependant.
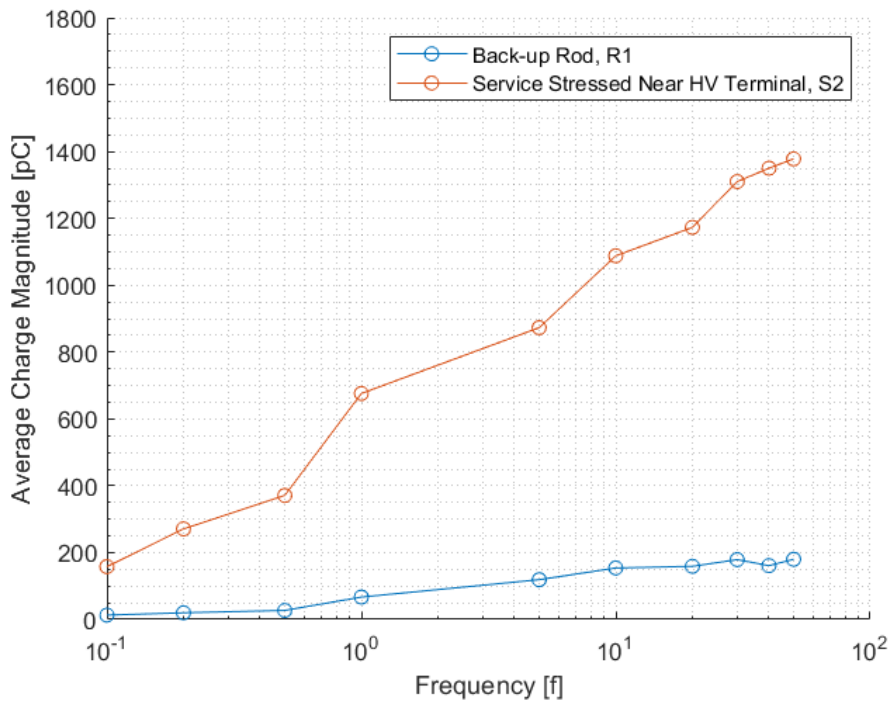
Figure 32: Average charge for rod R1 and S1 related to frequency.

5 Conclusion

The aim of this thesis was to apply techniques for detection and condition assessment for internal partial discharges in high voltage insulation. A theoretical estimation of two void shapes, cylindrical and spherical, based on electrical field distribution was performed. The FEM simulations was also considered in an analytical frequency dependency study by a capacitive and resistive ABC-model. At last an experimental laboratory test was conducted for a set of generator rods from a run-of-the-river power station in Norway, where its PD characteristics is discussed in relation to their performing condition.

From the results and the discussion given in this thesis the following conclusions can be made:

- The electric field in a cylindrical void is found the most homogeneous at void length 2mm and gap distance 0.2mm. This is the smallest size measured in this thesis, and this results is thus expected. However, as the gap distance is only at 10% of the void length with the small are of 0.4mm it is found that the edge effect is not present due to the very high overall field in the void. The same behavior is not found for any of the other void gap to void length, and it seems like this relation is strongly increasing with the void gap also increasing.

- The edge effect magnitude and affected area size seems to increase with a smaller area. With a void length of >10mm there is no longer a clear difference in the area affected by the edge effect. The magnitude of the electric field at the corners however seems to increase with an increasing length when the gap distance is fixed.

- For spherical cavities when the insulation is increasing accordingly with the void diameter, the electric field is following the theoretical limitation for spherical field given in Eq. 7. An exception was found with a void diameter and insulation layer thickness of 10mm. This can indicate that spherical dimensions over this limit does not fit with the theory given. It was also discussed that the model was under-dimensioned for for this insulation size as the total insulation thickness reached 30mm, the same thickness of the HV conductor in the FEM Model.

- The electric field of the spherical void when the insulation layers were not increased along with the void diameter, the electric field did not fit the theory in Eq. 7. As soon as the diameter increased over 1/3 in the size of the insulation thickness a deviation was proven. The deviation continued to grow larger as the void diameter reached the total thickness of the insulation layers.

- With the fixed void length and various lengths for the cylindrical void, it was clear that the void with the biggest area had the most homogeneous electric field. Studying the same dimensions under a frequency dependent study, it was clear that the inception voltage for each gap distance was not dependent on the frequency to some extent. A slight PDIV deviation under VLF was seen for all gap distances. For the biggest gap distance, 2.2mm, a 16% decrease in PDIV was observed for a VLF of 10^{-6}. For the max. apparent charge estimation n increase of 46% between the largest and smallest gap was found.

- An apparent charge estimation as the part of the analytical study of the FEM-voids was performed. This study shows that the smallest area, 0.2mm gap distance

with 2mm void yields the maximum apparent charge. The decrease of the apparent charge is proven by Equation 11.

- In the experimentally laboratory test conducted, 2 backup rods together with 2 service aged rod near HV was tested for PDIV and PDEV. For service rod S2, a clear deviation, from the average inception values of the other rods, was observed. S2 yielded a PDIV of 50% lower than for all the other rods, which was 500V under the generator operating conditions. From the rod data given, the rods had been in service for 40years, but it is not known if that rod have been replaced along the road. From a visual inspection of the rod, it was clear that some restoration have been conducted by the looks of the diamond connection of the bar-end. There were clearly large air gaps between the conductors, and some air was observed in the cross section into the groundwall insulation. However, it is hard to conclude that these voids go deep enough to pass the field grading paint into the rod. Hence, it is not known if these void affects the PDIV.
  When fitting the experimental measured PDIV to the ABC-model, the lowest PDIV found was at 2.9kV with a void distance of 1.9mm. This is close to equal to the PDIV of the 3 rods yielding the same PDIV while the model did not fit for service rod S2.

- The average charge magnitude was collected for one back up rod, and service rod S2. The results clearly shows that we are able to tell the rods apart based on the charge magnitudes for each frequency. The highest deviation between the two rods is found at the highest frequency tested, 50Hz.
  The increase of charge magnitude for each rod is equal to each other and it is concluded that for both of the conditions they are equally frequency dependant.

6 Further Work

- The original plan for this thesis before Covid-19 hit, was to have a complete experimental laboratory analysis of the given generator rods from the run-of-the-river power plant. Because of the school closing this was no longer an option, and an alternative approach of PD condition assessment was conducted. It would still be interesting to perform a thoroughly condition assessment for all 8 test objects given, including a thermal behavior analysis in respect to various frequencies.

- For all analytical tests in this thesis the same permittivity of polycarbonate have been used. For future work it would be interesting to look for the PD characteristics for other insulation materials to look for deviation from the theory we know.

- It is possible to analyse a variety of void dimensions of shapes, other than spherical and cylindrical which was presented in this thesis. This can give us a greater understanding of how the electric field unfolds under different parameters of various insulation materials.

- As it was clear that one of the serviced age generator rods had a lower inception voltage than the other, it would be interesting to find which characteristic of the rod is causing this. One suggestion is to remove the end diamond connection to compare the PDIV behavior. The length of the field grading paint should also be considered, along with any sharp edges on the copper electrodes.

References

[1] Torstein Aakre, E. Ildstad, Sverre Hvidsten, and Arne Nysveen. Review of partial discharge and dielectric loss tests for hydropower generator bars. *Proceedings of the Nordic Insulation Symposium*, 10 2017.

[2] Erling Ilstad. Tet4160 insulating materials for high voltage applications. *NTNU*, 2018.

[3] T. M. Sneve. "aldersfordeling for komponenter i kraftsystemet, levetid og behov for reinvesteringer. *NVE, 8, 2005*.

[4] Torstein Grav Aakre. Partial discharges in voids at variable voltage frequency and temperature diagnostic testing of stator mainwall insulation. *Doctoral theses at NTNU;2020:143*, May 2020.

[5] CIGRE wokring group A1.10. "survey of hydrogenerator failures. 2009.

[6] G. Stone, I. Culbert, E. Boulter, and H. Dhirani. *"Electrical insulation for rotating machines: design, evaluation, aging, testing, and repair"*. WILEY, 2nd edition, 2014.

[7] M. Farahani, H. Borsi, E. Gockenbach, and M. Kaufhold. Partial discharge and dissipation factor behavior of model insulating systems for high voltage rotating machines under different stresses. *IEEE Electrical Insulation Magazine*, 21(5):5–19, Sep. 2005.

[8] Jens R. Davidsen. "start/stopp problematikk; kjøremønsterrelaterte kostnader for vannkraftverk. *Statkraft, EBL Maskinteknisk Forum Wales, 2008*.

[9] George J. Anders, J. M. Boyd, Joseph M. Braun, Rostami Mina, Shyng her Lin, J. J. Liska, B. A. Lloyd, L. Mannik, Howard G. Sedding, and Greg C. Stone. Motor and generator insulation life estimation. 1992.

[10] W. McDermid. Development of a recommended practice for the measurement of pd from stator coils and bars. In *2015 IEEE Electrical Insulation Conference (EIC)*, pages 362–363, June 2015.

[11] C. Forssen and H. Edin. Partial discharges in a cavity at variable applied frequency part 1: measurements. *IEEE Transactions on Dielectrics and Electrical Insulation*, 15(6):1601–1609, December 2008.

[12] T. G. Aakre, E. Ildstad, and S. Hvidsten. Partial discharge inception voltage of voids enclosed in epoxy/mica versus voltage frequency and temperature. *IEEE Transactions on Dielectrics and Electrical Insulation*, 27(1):214–221, Feb 2020.

[13] Uno Gafvert, Hans Edin, and Cecilia Forssen. Modelling of partial discharge spectra measured with variable applied frequency. volume 3, pages 839 – 842 vol.3, 07 2003.

[14] M. Farahani, H. Borsi, and E. Gockenbach. Dielectric response studies on insulating system of high voltage rotating machines. *IEEE Transactions on Dielectrics and Electrical Insulation*, 13(2):383–393, 2006.

[15] Hazlee Illias, George Chen, and Paul Lewin. Modelling of partial discharge behaviour in a spherical cavity within a solid dielectric material as a function of temperature. pages 1 – 4, 11 2010.

[16] L. Niemeyer. A generalized approach to partial discharge modeling. *IEEE Transactions on Dielectrics and Electrical Insulation*, 2(4):510–528, Aug 1995.

A List Of Equipment

Equiptment	Specifications
Data Aqusition Unit	OMICRON MPD600
Power Supply	OMICRON MPP600
Measuring Impedance	OMICRON CPL542
Control Unit	OMICRON MCU502
High Voltage Amplifier	Trek Model 20/20B
Digital to Analog Converter	National Instruments NI USB 6216
Low Pass Filter	
Coupling Capacitor	3.4nC
Battery for Data Aquistion	Biltema 12V, 74Ah

B Importing Data from Comsol to MATLAB

```matlab
1  clc
2  clear all
3
4  folder = 'Folder Location on computer';          % Data location
5
6  ph = importPhData(folder,'unit1.1');             % Import phase
       vector
7  [t,q] = importQData(folder,'unit1.1');           % Import time
       and charge vector
8  [tv,v] = importVData(folder,'unit1.1');          % Import voltage
       timestamp and voltage amplitude
9
10 v = v - mean(v);
11 %Plot Discharges in relation to phase and voltage
12 figure
13 yyaxis left
14 plot(tv,v)
15 ylim(max(abs(v))*1.1*[-1,1])
16 xlabel('Time[s]')
17 ylabel('Voltage[V]')
18 yyaxis right
19 plot(t,q,'.')
20 ylim(max(abs(q))*1.1*[-1,1])
21 ylabel('Charge[q]')
22 legend({'z = Voltage','y = PD'},'Location','southwest')
23
24
25 %VoltageAdjustment = MeasuredVoltage/adjustVoltage(frekvens);
26
27 %fase= adjustPhase(0.1);
28
29
30 %%%
31 % Funksjoner under
32 %%%
33
34 function [v_tm, v] = importVData(folder, vUnit)
35
36 fileName = sprintf('%s\\%s.V', folder, vUnit);
37
38 file = fopen(fileName, 'rb');
39
40 if file == -1
41    msg = sprintf('file %s could not be opened', fileName);
42    error(msg);
43 end
```

```matlab
44
45  fseek(file, 0, 'bof');
46  v = fread(file, inf, 'float32');
47  v_tm = 48e-6 * (0:size(v, 1) - 1);
48
49  end
50
51  function [q_tm, q] = importQData(folder, qUnit)
52
53  fileName = sprintf('%s\\%s.Q', folder, qUnit);
54
55  file = fopen(fileName, 'rb');
56
57  if file == -1
58      msg = sprintf('file %s could not be opened', fileName);
59      error(msg);
60  end
61
62  fseek(file, 0, 'bof');
63  q = fread(file, inf, 'float32', 8);
64  fseek(file, 4, 'bof');
65  q_tm = fread(file, inf, 'float64', 4);
66
67  end
68
69  function phase = importPhData(folder, qUnit)
70
71  fileName = sprintf('%s\\%s.PH', folder, qUnit);
72
73  file = fopen(fileName, 'rb');
74
75  if file == -1
76      msg = sprintf('file %s could not be opened', fileName);
77      error(msg);
78  end
79
80  fseek(file, 0, 'bof');
81  phase = fread(file, inf, 'float64');
82  end
83
84  function k = adjustVoltage(frequency)
85      % k = 0.0164./frequency.^1.7420+1.06;
86      Param = [3.4e-9 9.5e10 30e-6 34303];
87      k = 1.009*8580*sqrt(1+(2*pi()*frequency*Param(1)*Param(2))
           .^2)./sqrt((1+Param(2)/Param(4))^2+(2*pi()*frequency*(
           Param(1)+Param(3))*Param(2)).^2);
88  end
89
```

```matlab
function Dphi = adjustPhase(frequency)
    Dphi = 1/(2*pi())*atan(1./(2*pi()*frequency*1.0291));
end
```

C PDIV estimation from ABC-model in MATLAB

```matlab
1  clc
2  clear all
3
4  format long
5
6  epsilonr =3.4;            %Relative permittivity of insulation
       material
7  epsilon0= 8.85*10^-12;
8  D=0.25;                   %Total insulation thickness
9  d=0.05;                   %Void gap distance
10 sigmab=2*(10^(-16));      %Conductivity of insulation material
11 sigmac=0;                 % Conductivity of the void
12 Uvoid= (6.72*(sqrt(d))+(24.36*d))/ sqrt(2) *1000;   %Paschen
13
14 j=0;
15 for f =0.00001:0.2:50 %Frequency range
16     j=j+1 ;
17
18     Ui=Uvoid*(1+(D/d)*((sigmac+2*pi*f*epsilon0)/(sigmab+2*pi*f*
          epsilon0*epsilonr)));
19
20     s_Ui(j)=Ui
21     s_f(j)=f
22
23
24 end
25
26 %Plot
27 hold on
28 plot(s_f ,s_Ui)
29 grid minor
30 set(gca, 'XScale', 'log')
31 ylim([0 10000])
32 xlabel('Frequency [Hz]')
33 ylabel('Voltage Ui[V]')
34 hold off
```